UNCLASSIFIED

AD NUMBER

ADB006121

NEW LIMITATION CHANGE

TO

Approved for public release, distribution unlimited

FROM

Distribution authorized to U.S. Gov't. agencies only; Test and Evaluation; MAY 1975. Other requests shall be referred to Commander, Air Force Armament Laboratory, Attn: DLMQ, Eglin AFB, FL 32542.

AUTHORITY

USADTC ltr, 5 Jun 1979

THIS PAGE IS UNCLASSIFIED

THIS REPORT HAS BEEN DELIMITED
AND CLEARED FOR PUBLIC RELEASE
UNDER DOD DIRECTIVE 5200.20 AND
NO RESTRICTIONS ARE IMPOSED UPON
ITS USE AND DISCLOSURE.

DISTRIBUTION STATEMENT A

APPROVED FOR PUBLIC RELEASE;
DISTRIBUTION UNLIMITED.

AFATL-TR-75-79

EFFECT OF MIXTURE RATIO ON UV, VISIBLE AND INFRARED RADIATION FROM EXHAUST PLUMES

TARGETS BRANCH
GUIDED WEAPONS DIVISION

AD B006121

DDC
RECEIVED
AUG 28 1975
B

AU NO.
DDC FILE COPY

MAY 1975

FINAL REPORT: JULY 1974 - MAY 1975

Distribution limited to U. S. Government agencies only; this report documents test and evaluation; distribution limitation applied May 1975 . Other requests for this document must be referred to the Air Force Armament Laboratory (DLMQ), Eglin Air Force Base, Florida 32542.

AIR FORCE ARMAMENT LABORATORY
AIR FORCE SYSTEMS COMMAND • UNITED STATES AIR FORCE
EGLIN AIR FORCE BASE, FLORIDA

Best Available Copy

UNCLASSIFIED

SECURITY CLASSIFICATION OF THIS PAGE (When Data Entered)

REPORT DOCUMENTATION PAGE

READ INSTRUCTIONS BEFORE COMPLETING FORM

1. REPORT NUMBER: AFATL-TR-75-79
2. GOVT ACCESSION NO.
3. RECIPIENT'S CATALOG NUMBER

4. TITLE (and Subtitle): EFFECT OF MIXTURE RATIO ON UV, VISIBLE AND INFRARED RADIATION FROM EXHAUST PLUMES.

5. TYPE OF REPORT & PERIOD COVERED: Final Report. 1 July 74 through 1 May 75

6. PERFORMING ORG. REPORT NUMBER

7. AUTHOR(s): D. B. Ebeoglu, C. W. Martin

8. CONTRACT OR GRANT NUMBER(s): 1921 03

9. PERFORMING ORGANIZATION NAME AND ADDRESS: Targets Branch (DLMQ), Air Force Armament Laboratory, Eglin Air Force Base, Florida 32542

10. PROGRAM ELEMENT, PROJECT, TASK AREA & WORK UNIT NUMBERS: Project No. AF- 1921, Task No. - 03, Work Unit No. - 001

11. CONTROLLING OFFICE NAME AND ADDRESS: Air Force Armament Laboratory, Armament Development and Test Center, Eglin Air Force Base, Florida 32542

12. REPORT DATE: May 1975

13. NUMBER OF PAGES: 64p.

14. MONITORING AGENCY NAME & ADDRESS (if different from Controlling Office)

15. SECURITY CLASS. (of this report): UNCLASSIFIED

15a. DECLASSIFICATION/DOWNGRADING SCHEDULE

16. DISTRIBUTION STATEMENT (of this Report): Distribution limited to U. S. Government agencies only; this report documents test and evaluation; distribution limitation applied May 1975. Other requests for this document must be referred to the Air Force Armament Laboratory (DLMQ), Eglin Air Force Base, Florida 32542.

17. DISTRIBUTION STATEMENT (of the abstract entered in Block 20, if different from Report)

18. SUPPLEMENTARY NOTES

Available in DDC

Best Available Copy

19. KEY WORDS (Continue on reverse side if necessary and identify by block number)

Plume Infrared Radiation Levels	Graybody Radiation
Infrared Interferometer Data	C_3 Radiation
Infrared Threat Signature Simulation Techniques	Stoichiometry
General Hydrocarbon Exhaust Plumes	Band Radiation
Oxidizer to Fuel (O/F) Ratio	Emission Mode

20. ABSTRACT (Continue on reverse side if necessary and identify by block number)

The development of infrared plume generators for aerial targets with the design goals of approximating threat aircraft/missile signatures required the identification of major physical and chemical parameters which affect the radiation characteristics (spectral and spatial intensity) of jet aircraft and missile exhaust plumes. Investigations have been carried out to determine the spectral distributions of general hydrocarbon exhaust and combustion between 0.3 and 14 microns. Gaseous, liquid and solid propellants, including pyrophorics, have been studied in the

DD FORM 1 JAN 73 1473 EDITION OF 1 NOV 65 IS OBSOLETE

400 936

UNCLASSIFIED

SECURITY CLASSIFICATION OF THIS PAGE (When Data Entered)

20. ABSTRACT (Concluded)

laboratory at static altitudes up to 18.3 kilometers (60,000 feet). The data show all hydrocarbons to have common major radiating species. In the infrared, the predominant radiating species at any oxidizer to fuel (O/F) ratio are always CO_2 and H_2O. In the ultraviolet and visible, the radicals of C_2, CH, and OH are the primary contributors to radiation from low O/F ratios to beyond stoichiometry. Band radiation at high mixture ratios is mainly due to OH. C_3 radiation is apparent at very fuel-rich conditions, although continuum, or graybody radiation, is the primary emission mode. One major parameter, O/F ratio, has been found to be the dominant factor affecting radiation at any wavelength. The data indicate propellant chemistry to have a relatively minor effect on infrared radiation levels. Afterburning has been determined to be the major radiation mechanism for low O/F plumes at static conditions.

PREFACE

This technical report describes the results of experiments and analyses performed by the Targets Branch (DLMQ) of the Air Force Armament Laboratory, Eglin AFB, Florida, in support of Program Element Number 62602F. Project Number 192103, entitled "Infrared Plume Simulation Technology." The investigations were conducted by Dr. D. B. Ebeoglu, Dr. R. T. Schneider, Lieutenant C. W. Martin, Mr. J. A. Knaur, Mr. A. J. Martellaro, and Mr. D. E. Fink. Professor Schneider (University of Florida), Mr. Knaur (Auburn University) and Mr. Martellaro (University of West Florida) carried out their work during the period June 1974 to October 1974 under temporary appointments to the Air Force Armament Laboratory. The infrared interferometer data were obtained and reduced by Captain W. B. Jollie (ADTC/TSGPA). Applications of the data described in this report, relevant to infrared countermeasures, have been presented to the 13th Infrared Information Symposium (IRIS) on Targets and Countermeasures, 8 through 10 April 1975, at Monterey, California, as a paper entitled "Spectral Distribution of Pyrophorics from 2 to 14 Microns" and is being published by the sponsoring organization. This effort was conducted during the period 1 July 1974 through 1 May 1975.

This technical report has been reviewed and is approved for publication.

FOR THE COMMANDER

JOHN W. JOHNSON
Deputy Chief, Guided Weapons Division

ABSTRACT

The development of infrared plume generators for aerial targets with the design goals of approximating threat aircraft/missile signatures required the identification of major physical and chemical parameters which affect the radiation characteristics (spectral and spatial intensity) of jet aircraft and missile exhaust plumes. Investigations have been carried out to determine the spectral distributions of general hydrocarbon exhaust and combustion between 0.3 and 14 microns. Gaseous, liquid and solid propellants, including pyrophorics, have been studied in the laboratory at static altitudes up to 18.3 kilometers (60,000 feet). The data show all hydrocarbons to have common major radiating species. In the infrared, the predominant radiating species at any oxidizer to fuel (O/F) ratio are always CO_2 and H_2O. In the ultraviolet and visible, the radicals of C_2, CH, and OH are the primary contributors to radiation from low O/F ratios to beyond stoichiometry. Band radiation at high mixture ratios is mainly due to OH. C_3 radiation is apparent at very fuel-rich conditions, although continuum, or graybody radiation, is the primary emission mode. One major parameter, O/F ratio, has been found to be the dominant factor affecting radiation at any wavelength. The data indicate propellant chemistry to have a relatively minor effect on infrared radiation levels. Afterburning has been determined to be the major radiation mechanism for low O/F plumes at static conditions.

SECTION I

INTRODUCTION

A continuing program of exploratory development to determine the degree to which infrared parameters of a jet aircraft exhaust plume can be simulated by a subscale target is being carried out by the Air Force Armament Laboratory. Considerable attention has been given to the fundamental dynamics of plumes and the basic parameters that determine the source, intensity, spatial and spectral distribution of plume infrared radiation. The underlying requirement for this basic understanding has been the need to develop sources that can produce maximum infrared radiation with minimum payloads.

Comprehensive investigations were recently carried out[1] to determine whether state-of-the-art computer models could predict the conditions necessary for maximum plume radiation. These data showed numerous significant differences to exist between prediction and measurement. In order to understand the reasons for these discrepancies, and resolve them, a comprehensive spectroscopic analysis was undertaken. This analysis has provided a much better insight into the basic mechanisms that must prevail for the emission of maximum infrared radiation from plumes.

A medium resolution 1 meter Czerny-Turner spectrometer was used to observe at ultraviolet and visible wavelengths, ranging from 0.3 to 0.65 micrometers, emission bands and their fine structure due to molecular vibration and rotation. A 4 cm^{-1} resolution interferometer spectrometer was used to obtain infrared spectra between 2 and 14 micrometers. The exhaust plumes of a variety of gaseous, liquid, and solid oxidizer and fuel mixtures in various chambers and nozzle configurations were studied as were free burning flames. Data were obtained over a range of simulated static altitudes up to 18.3 kilometers (60,000 feet).

[1]Ebeoglu, D. B. and Martin, C. W., "Experimental Verification of Infrared Plume Predicitons for a Rocket Engine," AFATL-TR-74-191, Eglin AFB, FL, November 1974.

SECTION II

EXPERIMENTAL CONDITIONS

1. EXPERIMENTAL GEOMETRY

The measurements in this investigation were all conducted in a vacuum chamber at Eglin AFB at static altitudes ranging from sea level to 18.3 kilometers (60,000 feet) in the general geometry shown in Figure 1. The measurements up to 5 micrometers were performed through a calcium fluoride window approximately 15 centimeters in diameter and 1.5 centimeters thick installed in port number 2 approximately 1.3 meters above the outside floor level. The 3 to 14 micrometer measurements at altitude were made through a potassium chloride window approximately 76 millimeters in diameter and 8 millimeters thick installed in the same port. The sea level measurements were made without a window. The vacuum chamber and the kerosene/oxygen rocket engine[2] and the unchoked atomized exhaust nozzle[3] used in the measurements have been described earlier in detail.

Free burning flames were produced in a shallow (1 cm high by 30 cm in diameter) asbestos-lined pan. In those cases where hot metal might fall within the field of view of an instrument, a circular asbestos mask with an 8 cm diameter opening was used at least 2 meters away from the combustion to ensure that only radiation from flame emission would be observed.

The subscale kerosens/oxygen rocket engine was generally operated at a constant mass flow rate of 5.0 gm/second with the O/F ratio being varied from 1.5 to 6.0 producing chamber pressures around 4 kg/cm^2. Precautions were observed to avoid the accumulation of carbon or smoke inside the altitude chamber when operating at low mixture ratios.

2. VISIBLE AND ULTRAVIOLET MEASUREMENTS

2.1 Equipment and Configuration

A Jarrell-Ash 1.0 m focal length Czerny-Turner spectrometer was positioned parallel to the long axis of the altitude chamber with mirror optics being used to direct the radiation from the plume as shown in Figure 2. The optics were positioned on an optical bench in front of the spectrometer as illustrated. This mirror arrangement allowed the selection of a desired part of the plume (parallel to the plume axis) to be

---

[2]Long, J. F., Ebeoglu, D. B., and Harwell, K. E., "Infrared Plumes Test Facility Handbook," AFATL-TR-74-15, Eglin AFB, FL, January 1974.

[3]Ebeoglu, D. B. and Martin, C. W., "The Infrared Signature of Pyrophorics", AFATL-TR-74-92, Eglin AFB, FL, May 1974.

directed onto the entrance slit. In general, the image of a plume was placed vertically on the slit. Enough light entered the spectrometer and the line width was wide enough to see distinct lines and their dependence on distance from the exit plane. A slit width of approximately 40 microns was used.

The objective lens used for the visible part of the spectrum was an f/5.6, 135mm focal length camera lens. For the UV, an f/8, 250mm focal length quartz lens was used. The spectrometer has an internal moveable mirror to either deflect the spectrum to a film plane or to the exit slit for observation by a photomultiplier. Polaroid® Land-type 107 (ASA 3000) film was used in a camera back attached to the spectrometer for permanent records. An RCA 1P28 photomultiplier tube coupled to a scope or a microvoltmeter was used for rapid data collection.

2.2 Optical Alignment Calibration

The complete optical path including the configuration used for UV and visible optical alignment is shown in Figure 3. The image of an exhaust plume was placed vertically on the slit. Utilizing a small HeNe laser, reflections from optical surfaces were made to return coincident with the incoming light to align the optical axis. The alignment procedure was performed before each set of measurements.

With the laser leveled, the beam was aligned perpendicular to the axis of the exhaust plume or flame. From there it passed through the CaF_2 window as shown in Figure 3 and was directed onto the entrance slit by adjusting the two first surface mirrors. The double mirror arrangement rotated the image of the plume from horizontal to vertical as shown in Figure 2. The bottom mirror was adjusted to keep the beam on the slit and centered on the alignment dot of the second parabolic mirror of the spectrometer. The grating was turned to 6328Å to insure that the laser light emerged from the exit slit. This procedure assured that light along the main optical axis would pass from a plane through the plume to the spectrometer exit slit. An objective lens was then introduced and adjusted to maintain the laser light on the slit with reflections from its surfaces coincident with the incoming beam.

Wavelength calibration was obtained using a mercury reference. The reading on the spectrograph dial in Angstroms gave the wavelength, approximately, at the left side of the Polaroid® film frame (e.g., 5000Å on the dial produces 4990Å on the left side of the film). The dispersion was determined to be 9.74Å/mm. (Dispersion is defined as the image scale on the film plane in Angstroms per millimeter. With a dispersion of approximately 10Å/mm, a spectrum about 710Å wide is put into the narrower dimension of a frame of Polaroid® 107 film.) During the measurements, the far window was blocked and all lights were shut off to insure that only light from the exhaust or combustion arrived at the entrance slit.

3. INFRARED MEASUREMENTS

An interferometer spectrometer (Block Engineering, Inc., Cambridge, Massachusetts, Model 600) was used to measure the infrared spectral distributions between 2 and 14 micrometers. Two sets of detectors and appropriate optics were used to span and overlap the range of wavelengths investigated. Uncooled PbSe or cooled InSb, both with CaF_2 optics between 3 and 14 micrometers. All the measurements were made at a resolution of 4 cm^{-1}. The field of view of the interferometer system ranged from 1/4 degree to 15 degrees, depending on the purpose of the measurement.

The scanning rate was 16 scans/second and generally data were taken over a one second interval and averaged. Final spectra, including corrections for detector spectral response, were generated on the spot by an accessory mini-computer. The radiant intensity levels described in this report are all in relative units. The cited references should be used for information on absolute radiant intensity and radiation figures of merit for the various hydrocarbons discussed.

SECTION III

EXPERIMENTAL RESULTS

1. VISIBLE/UV SPECTRA

The primary objective was to determine the conditions under which major radiation changes occur in engine exhaust plumes at visible and ultraviolet wavelengths, relate these to infrared radiation, identify radiating species and, finally, establish major parameters which affect the intensity of radiation. In order to obtain a better understanding of the limits of such variations, flames were created and spectra studied over a wider set of conditions than those produced by a single engine exhaust. Thus, the relative combustion spectra of kerosene, propane, and a number of pyrophorics were also studies, approximately in the band between 3000Å and 6500A. Bandheads, major lines, and fine line structure of the bands were all identified by reference to three standard textbooks on the subject: Pearse and Gaydon[4] (1963), Gaydon and Wolfhard[5] (1970), and Herzberg[6] (1950).

1.1 Kerosene/Oxygen Rocket Engine Spectra

Visible/UV spectra were taken over approximately 30-centimeter lengths of the exhaust plume at a simulated static altitude of 12.2 kilometers to compare against previous infrared measurements. At this altitude there was clear separation between the shocks. Figure 4 gives an orientation reference for the exhaust plume axial cross section with respect to the band radiation spectra. This illustration should be helpful in relating spectra to position within the plume. Visible/UV radiation begins sharply at the first shock, shows an increase in intensity in traversing the shocks and tapers off in intensity after the last shock region. No measurable visible/UV radiation is apparent between the exit plane and the first shock.

---

[4]Pearse, R. W. B. and Gaydon, A. G., "The Identification of Molecular Spectra," John Wiley, New York, 1963.

[5]Gaydon, A. G. and Wolfhard, H. G., "Flames - Their Structure, Radiation and Temperature," Chapman & Hall, London, 1970.

[6]Herzberg, G., "Spectra of Diatomic Molecules," Van Nostrand, New York, 1950.

Each of the spectra of the kerosene/oxygen engine plume presented in this report were photographed on several pieces of film, each at the same exposure level. Film sections were then spliced diagonally at characteristic bandhead wavelengths. Figure 5 shows two spectra obtained over the visible band between 3700 and 6500 Angstroms at two positions across the plume. Figure 5(a) was taken across a plane just missing the shock region (see Figure 4 for reference) and shows that only band radiation is present in this axial plane. Figure 5(b) shows the spectrum across the exact center of the plume. In this axis, some continuum emission is observed, though only from the shocks, in addition to the emission bands.

Figure 5 was obtained with the engine running at an O/F ratio of 3.5, which is near stoichiometric for a kerosene/oxygen mixture. Except for variations in intensity, the same spectral structure is also apparent for mixture ratios of 3.5 or below. The spectra in Figure 5 are exclusively those due to the radicals of CH and C_2 (Swan and high pressure bands). The most intense lines are the CH bandhead at 4314Å and C_2 (Swan bandhead) at 5165Å. The 4050Å (comet-head) band of C_3 was not apparent at any mixture ratio between 1.5 and 6.0, either on film or in the photomultiplier tube output.

The intensity of the band radiation due to these two radicals were then investigated as a function of mixture ratio. The variation in photomultiplier tube output at the above two bandhead wavelengths is shown in Figures 6 and 7. In both cases an extremely sharp increase in band radiation intensity occurs as the O/F ratio is reduced below 3.5 (stoichiometry). This variation with O/F ratio is similar to that observed in molecular CO_2 emission in the infrared band between 4 and 5 microns, although the rate of increase in visible band radiation is much larger. The previously measured[1] infrared radiant intensity variation with mixture ratio is reproduced in Figure 8 to show the comparison.

The presence of strong C_2 and CH emission are indicators of fuel rich flame combustion. Their intensities begin to fall off below a mixture ratio of 1.8, as does the infrared radiant intensity, indicating that the threshold for carbon luminosity may have been reached. However, although carbon is visually evident in the exhaust of engine at these conditions, it is apparent that the amount is nonetheless not high enough to contribute significant infrared radiation.

The data thus show the maximum visible rocket engine radiation to be primarily due to external combustion. An increase in infrared radiation accompanies the increase in visible radiation, i.e., the increase in external combustion. The absence of graybody radiation in the infrared

---

[1] Ibid, p. 59.

spectrum at these conditions[1] is paralleled by the limited visible continuum observed only over the shock regions.

Figure 9 shows the spectrum along the central axis of the plume extended into the ultraviolet for an O/F ratio of 2.5. Another band, the emission spectrum of the OH bandhead at 3064Å shows up quite clearly. The other major OH band at 3428 is only faintly apparent. Figure 10 shows UV band spectra between 2500 and 3600A (recorded on film at a constant exposure level) as the engine mixture ratio is varied between 2 and 6. It is seen that the intensity of the UV band also increases as the O/F ratio is decreased; though, as Figure 11 shows for the 3064Å bandhead, the rate of increase is not as high as for C_2, CH or for the infrared radiant intensity between 4 and 5 micrometers.

OH radical was determined to be the only major plume emitter at visible and ultraviolet wavelengths for a couple of major conditions:

1. It is the primary emitter at high mixture ratios. Figure 12 shows the rocket engine emission over the entire UV/visible band for an O/F ratio of 6. Clearly OH radiation predominates; the CH bandhead at 4314Å and the continuum from the shocks are apparent, though at much lower levels. This emission mode is the cause of the characteristic blue plumes observed at high mixture ratios.

2. It is the primary visible/UV plume emitter beyond the region of the shocks. Figure 13 shows the emission along the central plume axis from a point past the last shock to 30 centimeters downstream, for an O/F ratio of 3.5. Here, as in Figure 12, OH emission dominates accompanied by lower level CH radiation at 4314Å and faint C_2 radiation in the 5800Å band. (Figure 13 also shows an instrument anomaly, a second order spectrum starting at 6128Å generated by the spectrometer. This apparent band disappears, however, when a piece of glass is placed in front of the lens, thereby proving its origin.)

The OH radical is the only product of combustion identified which gives measurable radiation in the ultraviolet or visible. None of the major molecular combustion products, such as H_2O, CO_2, CO, H_2 or O_2, some of which are primary infrared radiators, were observed to emit in the visible or ultraviolet. O/F ratio, as in the infrared wavelengths, is the predominant parameter affecting the intensity and spectrum of radiation in the UV.

---

[1] Ibid, p. 31 - 39.

1.2 Free Combustion Spectra

In order to determine the total range of line radiation spectra that can be produced by externally burning exhausts, a variety of liquid and gaseous fuels were combusted in a crucible and also mixed with oxygen within a torch or atomizing nozzle. Visible band radiation from kerosene, and two pyrophorics, TEA* and TNPA** burned in a crucible are illustrated in Figure 14. In contrast to the kerosene/oxygen rocket spectra, the film exposure was varied in these data in order to show up any existing weak band radiation.

This extremely fuel rich combustion is obviously dominated by continuum radiation. Only two relatively faint bands appear within the continuum (1) the elusive 4050Å (comet-head) band of C_3 which could not be observed at any O/F ratio in the range of the kerosene/oxygen rocket engine, and (2) the CH band head at 4314Å. These bands show up for all fuels combusted in this fashion.

The change in band radiation as the O/F ratio is varied from very fuel rich to very oxygen rich was studied by mixing the fuel with increasing amounts of oxygen. Figure 15 shows the UV and visible spectra for propane across a wide range of mixture ratios. At very fuel rich conditions (i.e., with the propane externally mixing with ambient air) the flame radiation is entirely similar to the spectra shown in Figure 14. As some oxygen is mixed with the propane the OH band at 3064Å begins to appear and continuum radiation appears to decrease.

At very oxygen-rich conditions the continuum decreases further and the OH line radiation intensity in the ultraviolet increases. The intensity of the second OH bandhead at 3428Å increases and other UV and visible emissions become insignificant. (Figure 5 also shows the second order spectrum noted in Figure 13.) Thus, at the two extremes of mixture ratio, combustion varies from a contiuum produced by carbon luminosity all the way to a purely ultraviolet emission. Intermediate conditions produce the C_2 and CH bands which result in a green/yellow plume.

Very similar spectra to those shown in Figure 15 were generated by a number of pyrophoric materials exhausted into static ambient conditions via an atomizing nozzle. The flow rate of nitrogen used to atomize the mixtures was varied in order to vary the length of the plumes and thus the mixing of the fuel with the ambient air. Although the solely ultraviolet radiation condition was never reached, the OH line radiation

---

*Tri-ethyl aluminum

**Tri-n-propyl aluminum

increase and continuum radiation decrease shown in Figure 15 were noted as the nitrogen flow rate was augmented, thus increasing the plume volume and consequently the air-to-fuel ratio of the secondary combustion.

2. INFRARED SPECTRA

The objective of the infrared measurements was to determine the variation in infrared spectra over the same range of conditions that produce the visible and ultraviolet spectra just described. The infrared spectral distribution between 2 and 5 micrometers for the kerosene/oxygen engine, over the range of O/F ratios between 1.5 and 6.0, has been described in detail previously[1]. The present data explore conditions beyond these.

The first set of measurements were taken at very fuel-rich conditions with materials burning freely in a crucible. Figures 16 through 19 show infrared spectra between 2 and 5 micrometers for kerosene and three pyrophorics, TEA, 60% DEAH*/40% TEA and DEAC**. As is evident, the spectra are very much identical and consist of a graybody spectrum and CO_2 and H_2O radiation. The gap between the blue and red spikes of CO_2 in the 4- to 5-micron band is small due to the short ranges at which the data were obtained. The DEAC spectrum (Figure 9) shows HCl lines as a minor fluctuation superimposed on the graybody spectrum between 3.5 and 3.8 microns.

The relative spectra emitted between 3 and 14 microns in a crucible burn similarly resemble each other. Figures 20 and 21 show the spectra for kerosene and 60% DEAH/40% TEA, respectively. Since the relative amount of radiation observed above 5 microns is so low, the region was divided into two parts for better examination. Figure 22 shows the spectrum between 3 and 9 microns and Figure 23 that between 5 and 14 microns for 60% DEAH/40% TEA.

It is apparent that the infrared spectrum beyond 5 microns is primarily due to the tail end of the graybody radiation which ends at about 6 microns. Some CO_2 and H_2O radiation is present between 6 and 9 microns. The radiation emitted between 9 and 14 microns, while being above background, is quite minimal. (The apparent reduction in the blue spike amplitude seen in Figures 20 and 21 is merely due to the performance of the x-y recorder--the amplitude is restored to normal proportions in narrower bandwidth displays such as in Figure 22).

These spectra differ from those obtained with the kerosene/oxygen engine at any O/F ratio. The latter do not exhibit graybody radiation as can be seen from the spectrum reproduced in Figure 24. The change in the infrared spectral distribution to graybody and, in the visible and

---

[1] Ibid, p. 6 - 40.

*Di-ethyl aluminum hydride
**Di-ethyl aluminum chloride

ultraviolet to continuum, occurs at extremely low O/F ratios where carbon or particulates are produced in sufficient quantity. It occurs with any hydrocarbon, although at different O/F ratios.

Figures 25 and 26 show the difference in the spectrum between 2 and 5 micrometers of a propane blow-torch at oxygen-rich and fuel-rich conditions, respectively. The former spectrum is emitted over a relatively wide range of mixture ratios. The spectrum shifts to that shown in Figure 26 only for very low O/F ratios (well below 1.0 for propane), when the combustion is extremely rich in carbon or particulates. The mere existence of carbon in a combustion, or in an exhaust, is not enough to change the infrared spectrum. Thus, the kerosene/oxygen rocket engine operated at an O/F ratio of 1.7, shown in Figure 24, where abundant carbon is observed in the plume (and indeed accumulates in the engine chamber) has a spectrum similar to that shown in Figure 25.

The engine of the high altitude supersonic target (HAST) (a hybrid rocket burning a mixture of solid polybutadiene and polystyrene and liquid inhibited red fuming nitric acid [IRFNA]), on the other hand, gives the spectrum shown in Figure 27, for an O/F = 3.0 (stoichiometry being an O/F $\approx$ 4.5), similar to those shown in Figures 16 through 19. This hybrid rocket engine emits this spectrum for a wide range of O/F ratios because its exhaust is laden with particulates at nearly all mixture ratios. The combustion of metallized solid propellant grains produce spectra ranging between those shown in Figures 16 through 19 and that shown in Figure 26 with some individual line spectra always appearing at amplitudes comparable to that of HCl in Figure 19. In general, though, the metal oxides, such as Al_2O_3, appear merely to add to the bulk of the graybody radiation.

Pyrophorics produce the same gamut of spectra. For example, 60% DEAH/40% TEA exhibits the spectrum shown in Figure 18 in a static free burn, the spectrum shown in Figure 28 when exhausted out of the atomizing nozzle at a low nitrogen pressure and, finally, the spectrum shown in Figure 29 as the nitrogen pressure is increased further. Increasing the amount of ambient oxygen mixing with the pyrophorics in this way results in the reproduction of the same spectral variations observed with other hydrocarbons. Figures 18, 28 and 29 thus represent almost the entire range of infrared that can be emitted by any hydrocarbon.

The range can be completed by examining the spectra of materials used for flares. These materials exhibit the graybody spectrum emitted by fuel rich hydrocarbon mixtures with the absence of CO_2 emission between 4 and 5 micrometers. Figures 30 and 31 show the spectrum of a slurry of heptane, sodium nitrate and magnesium at sea level and at a static altitude of 9.15 kilometers, respectively. Figure 30 shows that, at sea level, CO_2 radiation is not apparent. Assuming that it is emitted, its radiation is swamped by the graybody emitters. CO_2 radiation reappears when the same material is combusted at altitude, as shown in Figure 31.

It is postulated that the flame expands at altitude (increasing the ambient air/fuel mixture), accompanied by a relative decrease of graybody emission (as evident from the ratio of radiation emitted at lower bands), secondary combustion increases, and CO_2 radiation is produced. Flare materials that do not contain oxygen in their chemistry similarly exhibit CO_2 spectra when burned at static high altitudes, further pointing toward this postulated mechanism. The spectra for magnesium/Teflon® shown in Figures 32 and 33 combusted at a static 9.15 and 18.3 kilometers, respectively, show increasing CO_2 emission as altitude is increased and illustrate this point. These represent the extreme type of spectral emission from a hydrocarbon.

The infrared spectra to 14 microns are predictable extensions of these data. Fuel-rich combustion has been illustrated in Figure 20 by kerosene. Figure 34 shows the other extreme, an oxygen-rich exhaust; in this case, a propane torch between 3 and 14 microns. The kerosene/oxygen rocket engine exhibits the same spectrum in this band for any of the mixture ratios at which it can be operated. Radiation at 10.6 micrometers is minimal indicating laser action not to be a meaningful mechanism for CO_2 emission.

These data can be summarized as shown in Table 1 and the ratio of radiation in one band compared to that in another. CO_2 radiation between 4 and 5 microns which is common to all types of combustion, except some flares at some conditions, is normalized to 1.0. Expected relative radiation levels over other significant bands, 2 to 4, 5 to 9, and 9 to 14 microns, specifically, were obtained by integrating over the spectra.

TABLE 1. INFRARED RADIANT INTENSITY DISTRIBUTIONS
MATERIALS: TEA, DEAC, TNA, DIBAH, KEROSENE, PROPANE, ETC.

CONDITION	2-4 MICRONS	4-5 MICRONS	5-9 MICRONS	9-14 MICRONS
Fuel Rich (Crucible Burn)	1.7-3.7	1.0	0.4-0.6	0.1-0.2
Oxidizer Rich (Plume Burn)	0.02-0.1	1.0	0.05-0.15	0.02

3. SPATIAL DISTRIBUTION OF INFRARED VERSUS VISIBLE PLUME RADIATION

The relationship between the infrared and the visible exhaust plume of the kerosene/oxygen rocket engine can also be examined spatially to obtain insight into radiation mechanisms. Visible and IR images of plumes were, therefore, collected simultaneously.

Visible photographs were taken at two exposure settings in order to show the shocks as well as the extremities of the visible plume. The photographs of the entire visible plume were all taken at one exposure setting. In order to isolate the shocks, exposures were reduced all the way from a factor of 2 at an O/F = 6 to 550 at an O/F = 2. Type 107 (3000 ASA) Polaroid® film cuts off at 6500Å; thus this technique gave the very maximum boundaries of the visible radiation without including any of the near infrared.

The infrared plume was obtained between 4 and 5.5 micrometers with the BOFORS thermal scanner.[7] A Hewlett Packard Model 9830 general purpose computer was used to reduce both sets of images to a common x-y scale. The data were taken at a total mass flow rate of 5 grams/second, at a static altitude simulating 12.2 kilometers and over a number of mixture ratios.

Figures 35 through 39 show the contrast between the visible and the infrared plume spatial distribution (displayed to the same scale) as the O/F ratio is varied between 6 and 2. In all instances the infrared plume is larger than the visible and in all cases maximum infrared radiation occurs well downstream of the shock region. The position of the shocks, as well as the size of the shocks, are the same at visible and infrared wavelengths. The intensity of the shocks increases with decreasing mixture ratio.

Figure 40 shows a visible plume superimposed on a two-dimensional display of the infrared image wherein radiation intensity is represented by quasi-gray levels. These data were obtained at an O/F = 1.7 and a flow rate of 9 grams/second and correlates with the lower flow rate data. All the data show the size of the infrared plume to increase with decreasing O/F ratio much faster than does the visible plume.

---

[7]Martin, C. W., Askow, R. F., & Ebeoglu, D. B., "Operation of an Infrared Thermal Scanner for Plume Measurements," AFATL-TR-74-204, Eglin AFB, Florida, December 1974.

SECTION IV

CONCLUSIONS AND RECOMMENDATIONS

1. CONCLUSIONS

The combined spectral and spatial data show the rocket engine exhaust plume to be made up of three distinct radiation regions. As can generally be observed in the last set of figures, the first incorporates the shocks, the second extends to the end of the visible boundaries and the third encompasses the entire infrared plume. The variation of the radiation from these regions with mixture ratio, coupled with the interpretation of the spectral data, lead to significant conclusions on radiation from plumes in general and at static altitudes in particular.

a. The shock region is an ignition region. Line reversal temperature measurements conducted on the rocket engine plume show that the exhaust plume temperature from the exit plane up to the first shock is below 700°C. Extremely low infrared radiant intensity has similarly been noted in this region. Plume temperature increases significantly starting at the first shock as does infrared radiant intensity. It is believed that the first shock (as well as subsequent ones) act somewhat as spark plugs igniting and reheating unburned fuels or combustible gases which are exhausted at O/F ratios below stoichiometric. The shocks thus form an ignition region. This region initiates combustion in the plume and thus causes significantly increased radiation to be emitted by the plume.

b. The visible/UV region is a combustion region. The visible/UV spectra show external combustion to be the origin of most of the maximum radiation at these wavelengths. At high O/F ratios the infrared plume extends only slightly beyond the visible plume. At high O/F ratios visible/UV radiation from the plume is primarily due to the OH radical. The latter is simply a product of the combustion taking place inside the rocket engine chamber. As the O/F ratio is decreased, on the other hand, the sharp increase in C_2 and CH band radiation tends to point towards increased secondary combustion within the plume. The spatial data show this combustion to occur over an increasing volume as O/F ratio is decreased.

The cause for the increase in plume volume (and plume radiation) with decreasing O/F ratio is believed to be either partially combusted fuel or combustible gases from the exhaust interacting with the ambient oxygen in the air. Very little of the radiation produced within this combustion zone in the kerosene/oxygen rocket engine plume is continuum or graybody radiation. Thus it is doubtful that, in this case, combustion mechanisms involving carbon are directly involved.

The expansion of the combustion zone ends sharply when the O/F ratio is reduced further to a condition where either (a) the exhaust temperature drops with O/F ratio to the point where the unburned fuel or combustible

gases have difficulty combusting or (b) carbon is produced in sufficient quantity to suppress the radiation emitted by the plume. At low O/F ratios the combustion product, OH, dominates visible/UV radiation only at the extremities of the visible plume, indicating the end of the combustion zone and the beginning of the true exhaust.

c. The primary static plume radiation mechanism is afterburning. At static conditions, the radiation from the plume downstream of the visible region is all in the infrared. It is interesting to note that even though external burning, i.e., visible radiation and UV radiation from an exhaust product, has stopped, infrared radiation is still emitted. The radiating species remain CO_2 and H_2O. The data on plume geometry suggest that the infrared emission is possibly due to heated ambient air that is entrained by the high velocity plume.

The variation of infrared radiant intensity, J, or more specifically, $\bar{J}^*$, of the CO_2 band at 4 to 5 micrometers, with O/F ratio, shows the optimum O/F to shift with altitude. The lower the altitude, i.e., the more air in the ambient, the smaller the O/F ratio at which the maximum $\bar{J}$ occurs. The equivalent volume of the radiating plume increases as the O/F ratio is decreased, in much the same way as $\bar{J}$ increases, as illustrated in Figure 41. The approximate shape of the infrared plume goes from cylindrical at high O/F to conical at low O/F. The peak of the maximum infrared radiation occurs at a considerable distance from the exit plane. These observations all lead to the conclusion that the primary mechanism for infrared radiation, at static altitude conditions, is the external burning of either (a) combustible exhaust gases, (b) unburned fuel, or (c) both, with ambient air. This mechanism is, henceforth, defined as afterburning.

Afterburning is the primary radiation mechanism at static conditions above sea level; afterburning increases when the O/F ratio is decreased as more hot unburned fuel is released into the ambient environment, causing the large increase in radiant intensity noted at low O/F ratios.

d. Analytical prediction models do not treat afterburning adequately. Computer modeling predicts the radiant intensity from the kerosene/oxygen engine at static altitude conditions to vary with mixture ratio in the same manner as the engine chamber combustion temperature. The experimental data described here indicate strongly that the actual plume radiant intensity variation with mixture ratio is due to the rapid increase in afterburning as more hot combustible gas or unburned fuel is exhausted. This is a major mechanism which would tend to mask other flow fields and emission modes such as those predicted by the models. Although there may be additional reasons for the discrepancy between measurement and calculation, it would be highly unlikely that model validation could be achieved without first adequately incorporating the physical mechanism of afterburning into the calculations.

2. RECOMMENDATIONS

The first recommendation is to experimentally determine the contribution of afterburning to plume radiation in typical dynamic air flow environments. It is recommended that experiments be performed on the same engine in both air flow/altitude regimes and also with an inert gas (nitrogen) ambient. Measurements conducted at both these conditions would determine the contribution of afterburning and separate kinetic effects of air flow from the effects of afterburning. The final major variable, air flow, would be added to the matrix of parameters affecting maximum radiation from exhaust plumes and, at the same time, the contribution of afterburning as a radiation mechanism in a flight environment would be assessed.

The second recommendation is to reexamine the structure of computer models at static altitudes above sea level to determine to what extent afterburning is treated in the analysis and computations. Afterburning, as a radiation mechanism, must be considered at all the operational altitudes of aircraft and targets. Obviously, static conditions represent the worst case for radiation due to afterburning since entrainment is at a maximum and radiating gases are not dispersed away from the combustion zone by air flow.

The third recommendation is to exploit a major mechanism for maximum plume radiation that becomes apparent from the data presented in this report. Augmented radiation from a rocket engine plume is observed at any wavelength whenever combustion takes place in the plume itself. The corollary to this conclusion is that maximum radiation from a rocket engine plume will be produced whenever maximum combustion is produced in the plume. It is thus recommended that techniques be investigated to increase (a) emission of hot combustible gases from the exhaust and (b) increase combustion in the plume. It is recommended that these investigations be performed in a dynamic air flow environment as well as an inert environment in order to ascertain in-flight performance. The fundamental information described in this report on secondary combustion should thus be exploited to control plume size, shape, and structure to simulate full size threat engines by targets with subscale hardware.

(The reverse of this page is blank)

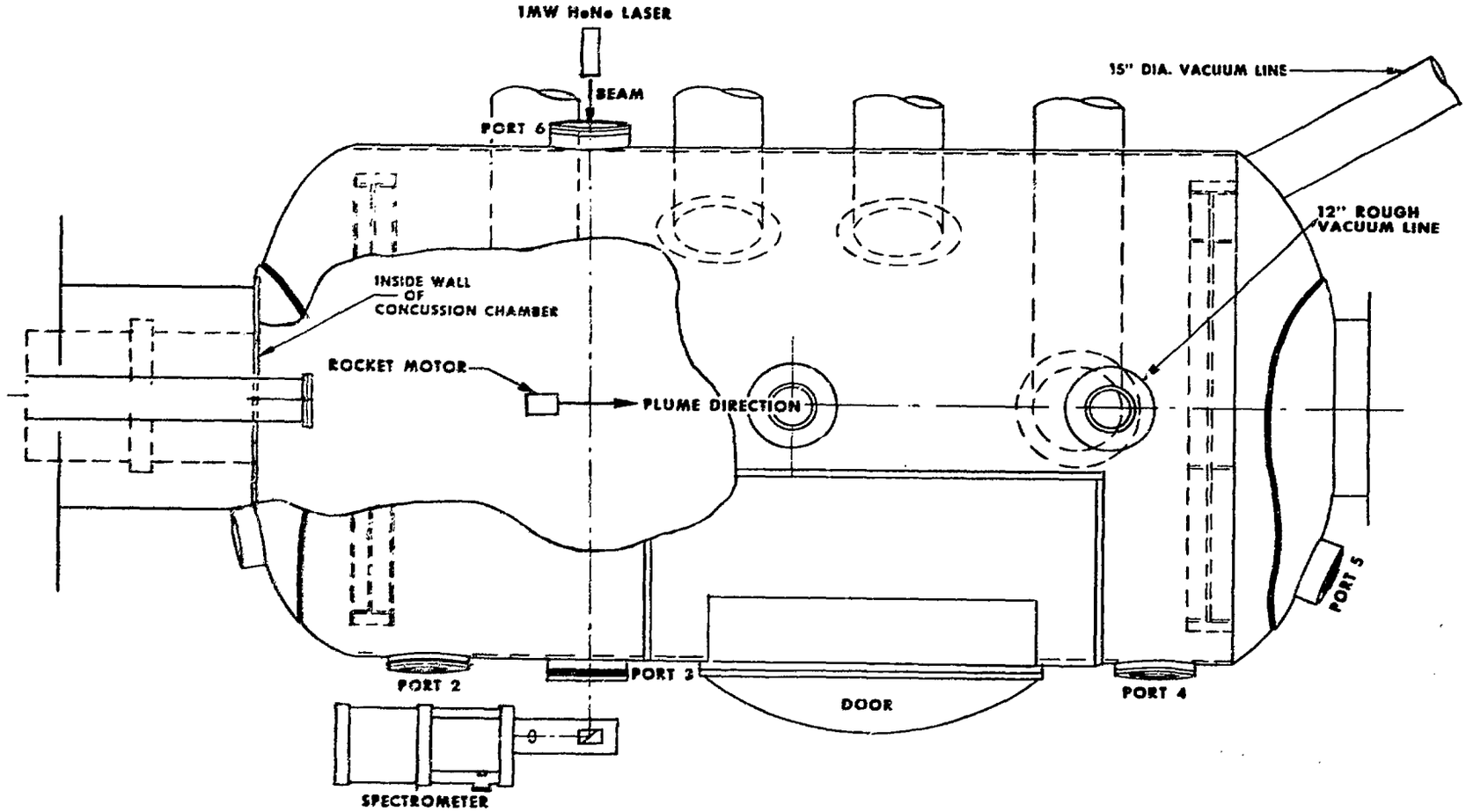

Figure 1. Experiment Configuration

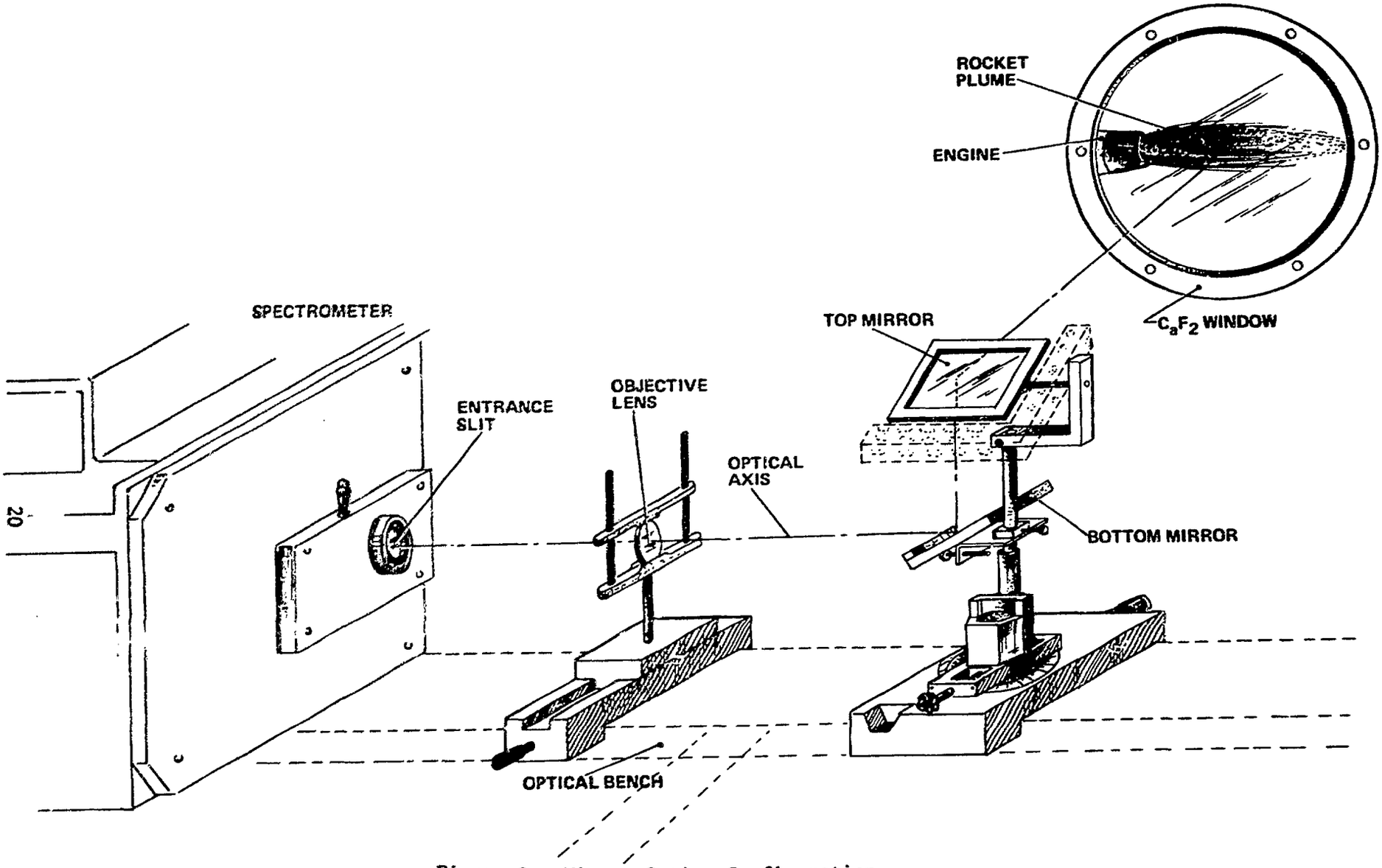

Figure 2. Mirror-Optics Configuration

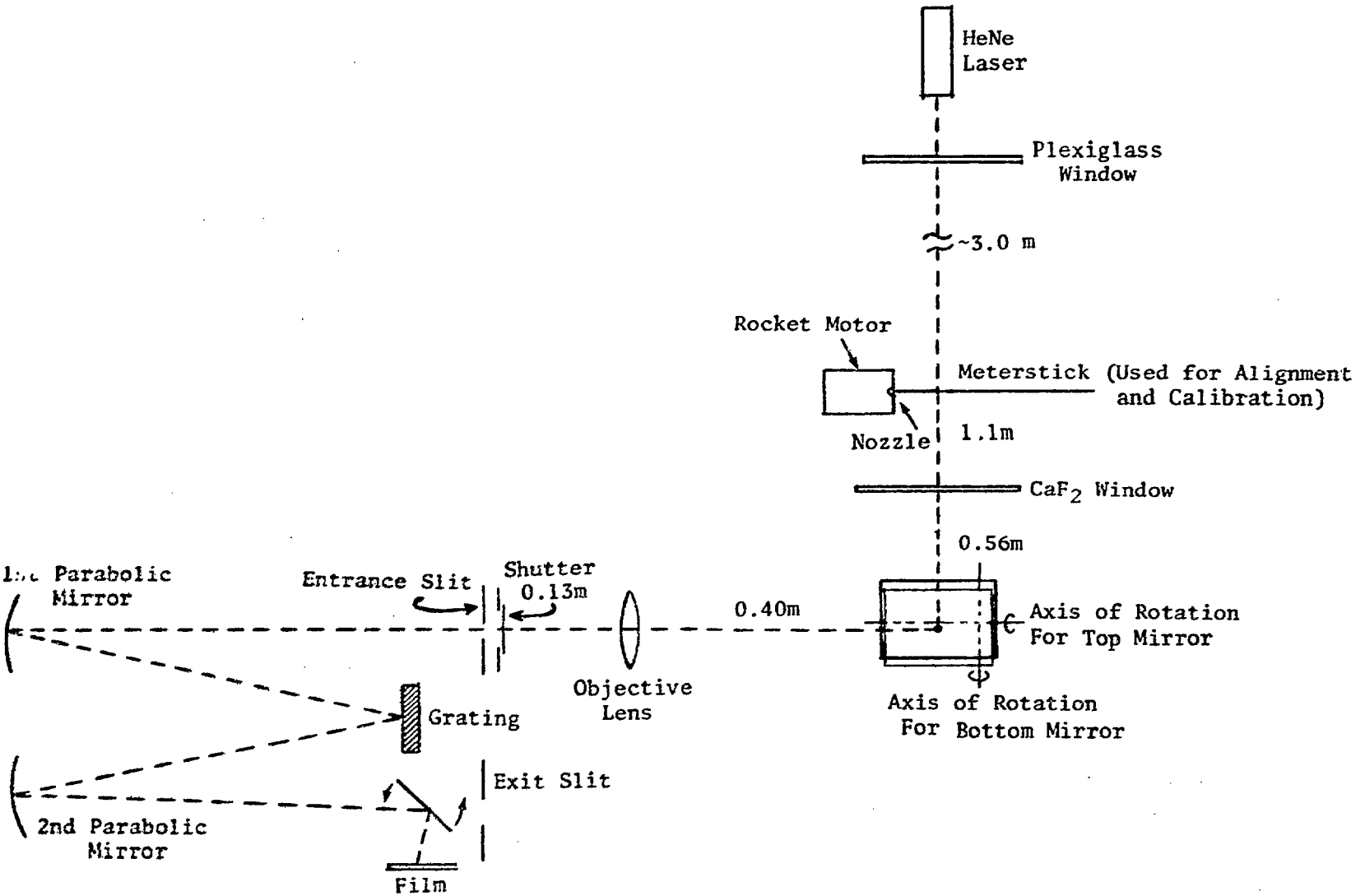

Figure 3. Complete Optical Path

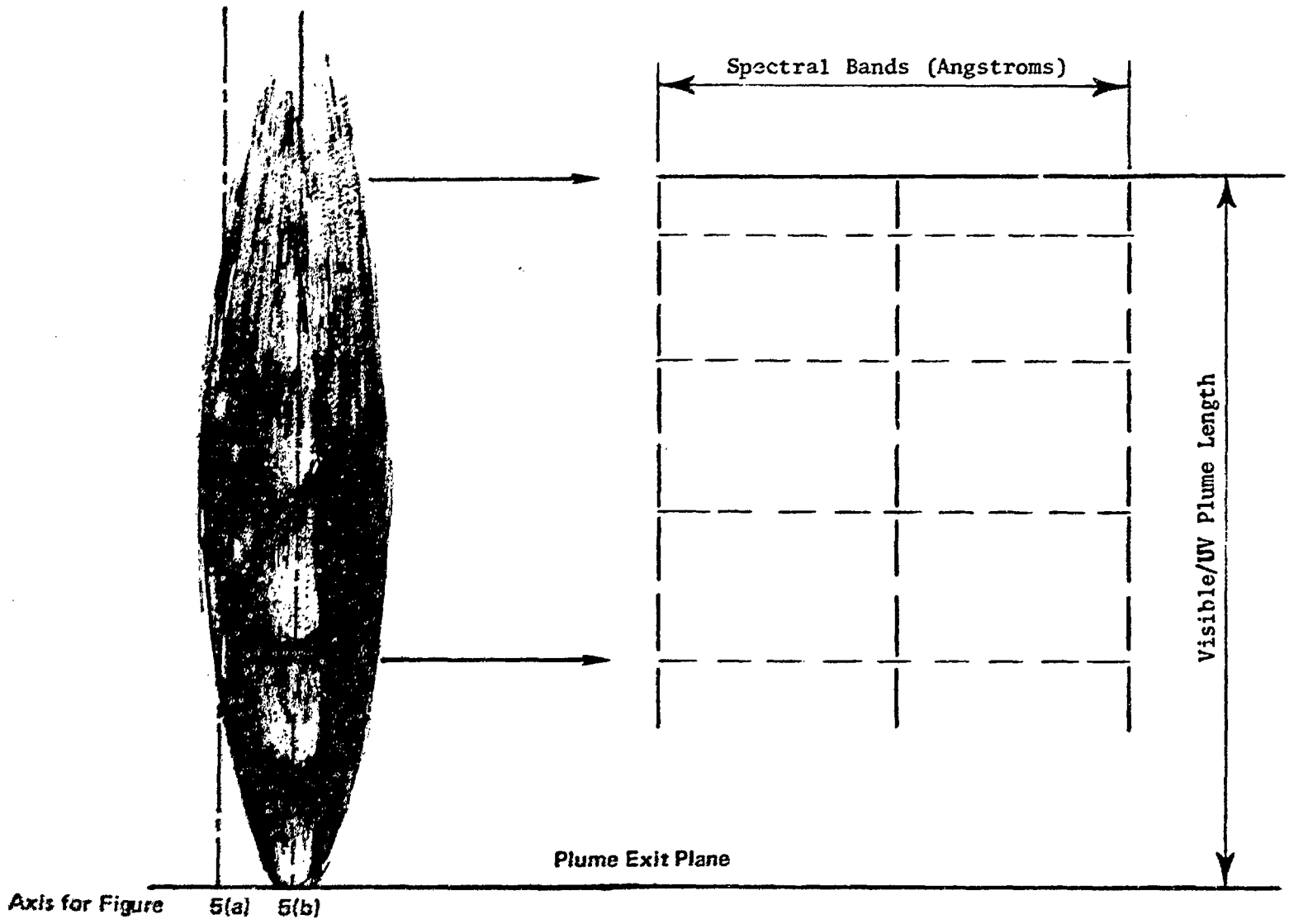

Figure 4. Reference Between Plume Orientation and Visible/UV Spectral Bands

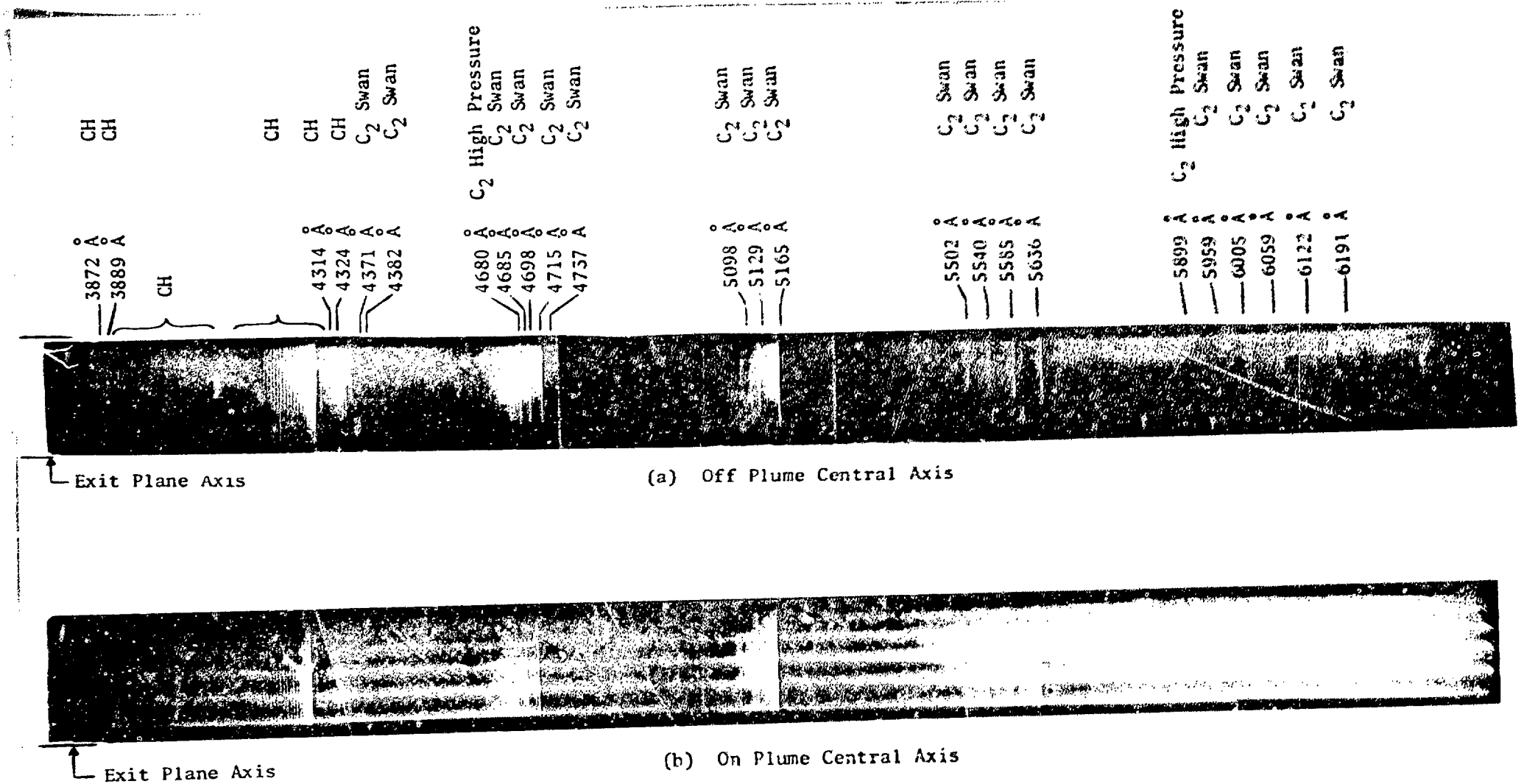

Figure 5. Visible Plume Radiation of Kerosene/Oxygen Engine at O/F = 3.5

(The reverse of this page is blank)

PRECEDING PAGE BLANK-NOT FILMED.

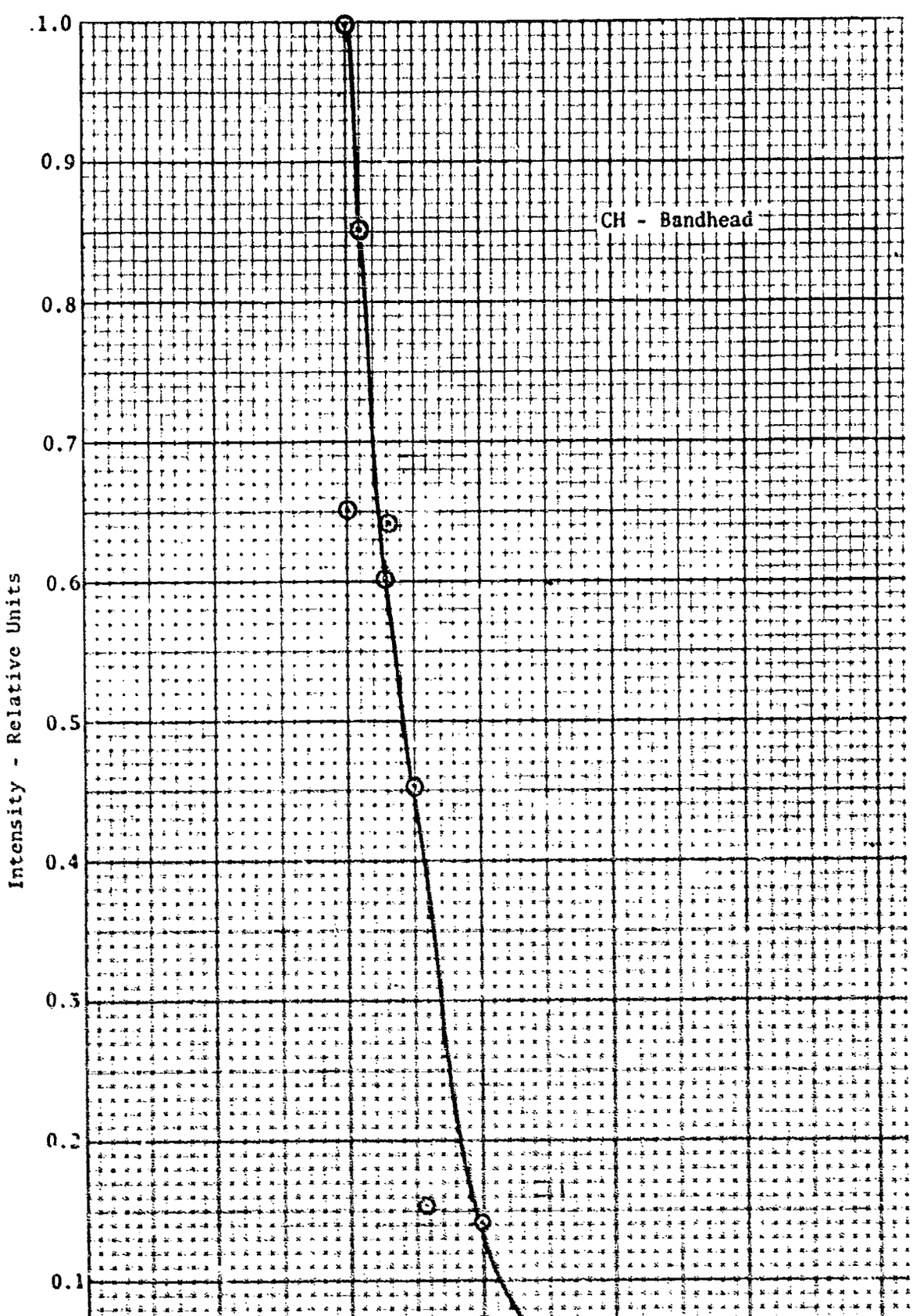

Figure 6. CH Radiation (4314Å Bandhead) Versus O/F Ratio

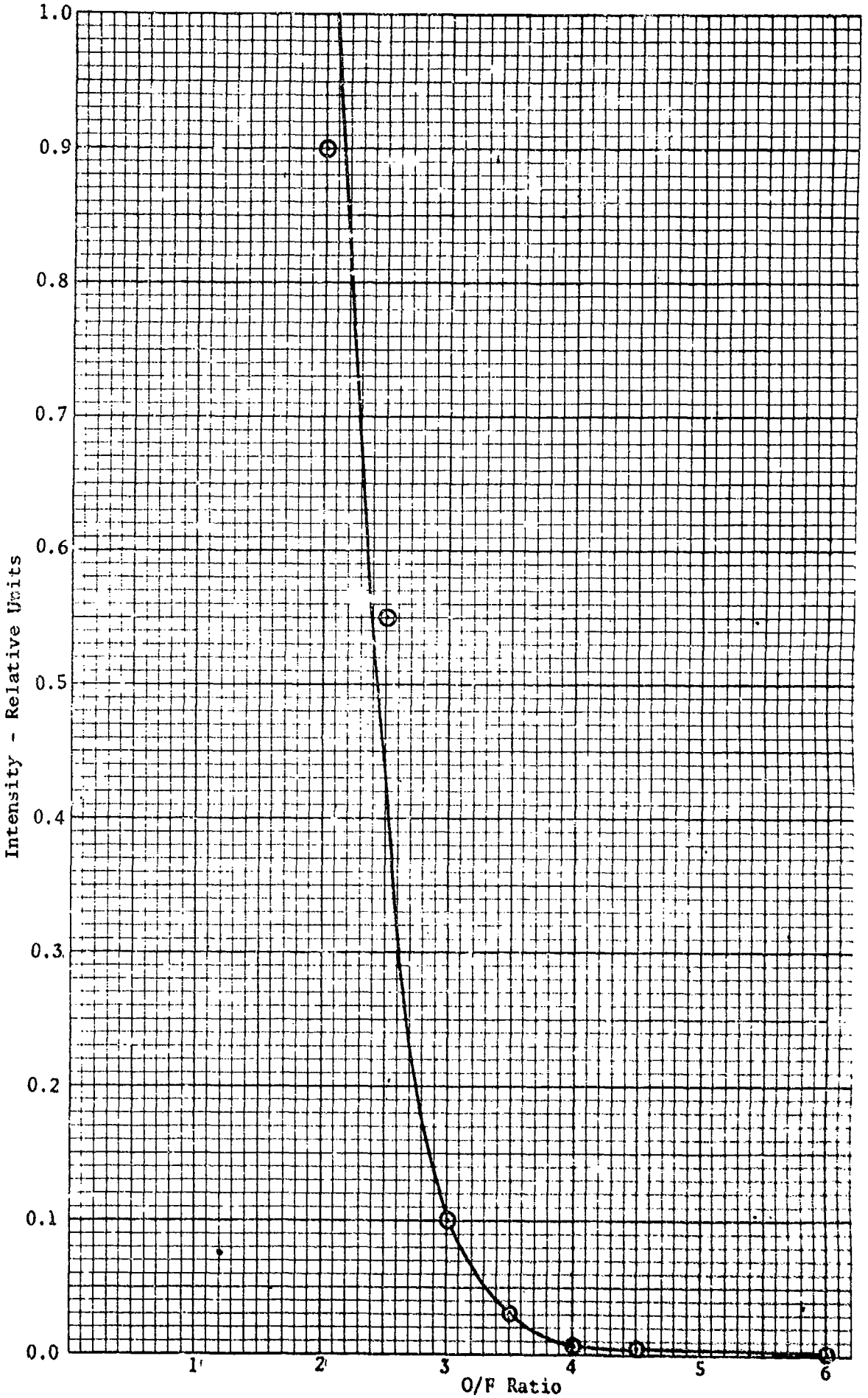

Figure 7. C_2 Radiation (5165Å Bandhead) Versus O/F Ratio

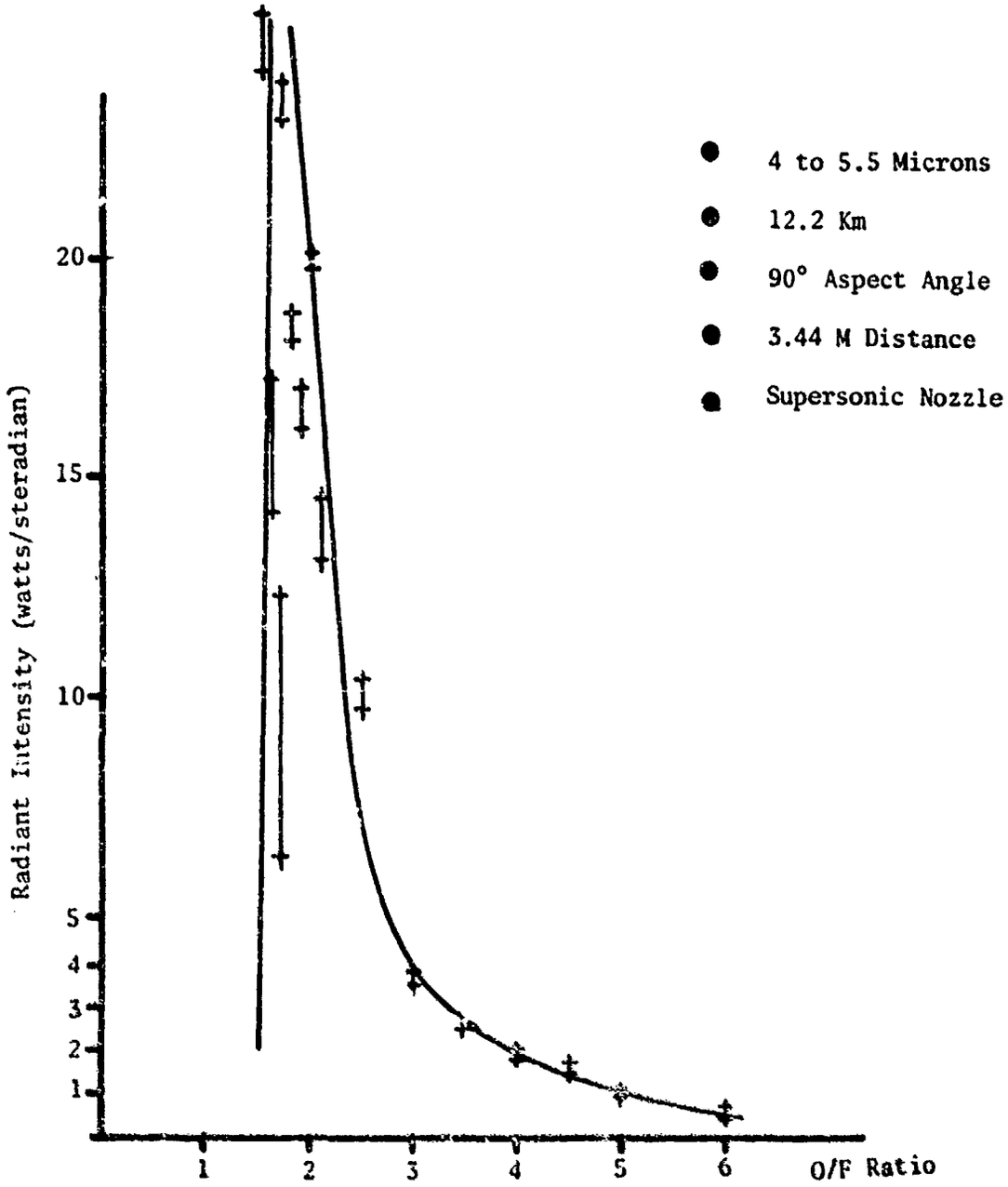

Figure 8. Infrared Radiant Intensity Versus O/F Ratio

(The reverse of this page is blank)

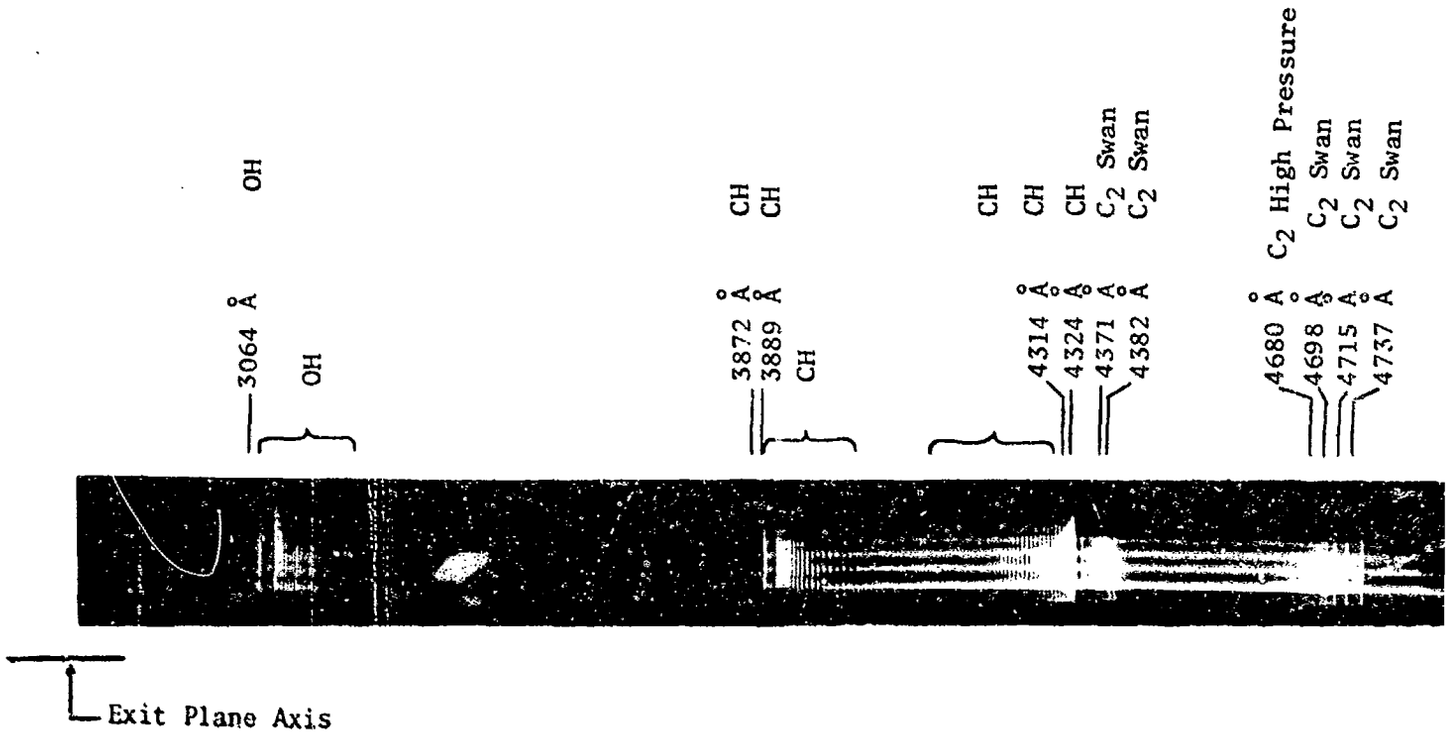

Exit Plane Axis

Figure 9. Visible/UV Plume Radiation of Kerose
(Central Axis

Radiation of Kerosene/Oxygen Engine at O/F = 2.5
(Central Axis)

(The reverse of this page is blank)

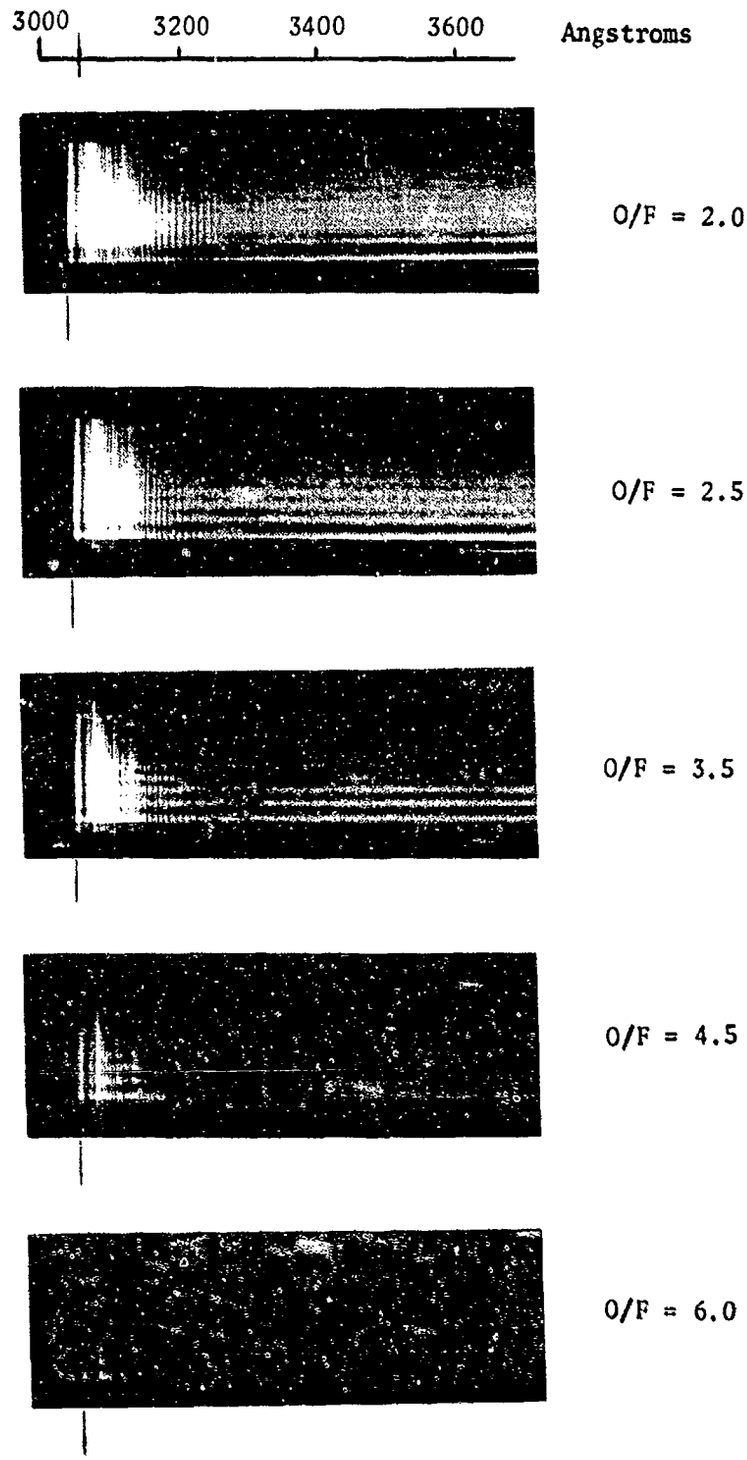

Figure 10. Ultraviolet OH Band Radiation Versus O/F Ratio (1 Minute Exposure)

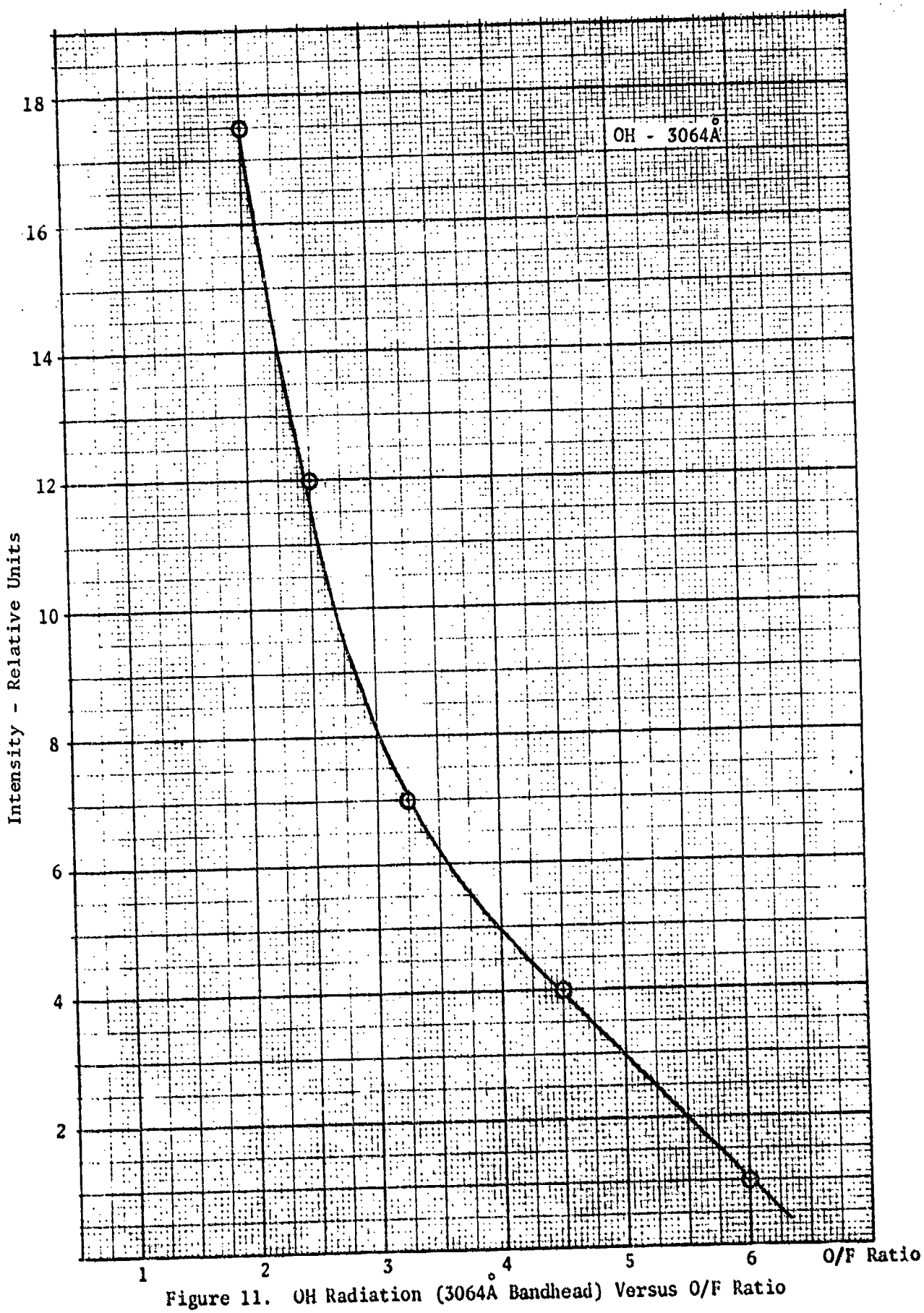

Figure 11. OH Radiation (3064Å Bandhead) Versus O/F Ratio

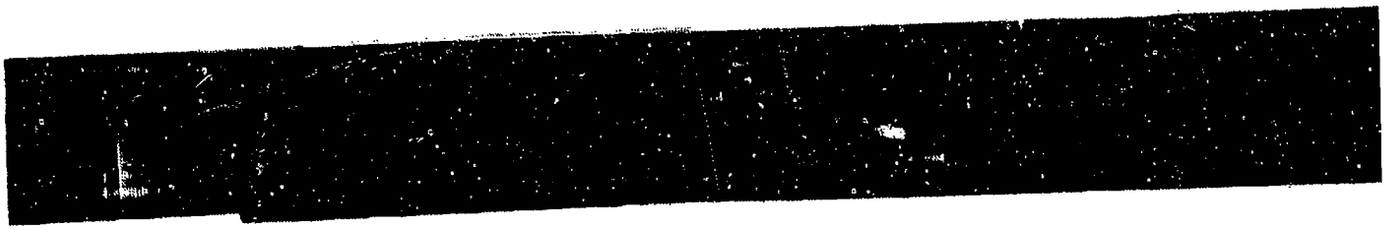

Figure 12. Visible/Ultraviolet Plume Radiation of Ker

Figure 13. Visible/Ultraviolet Plume Radia
(Central Axis -

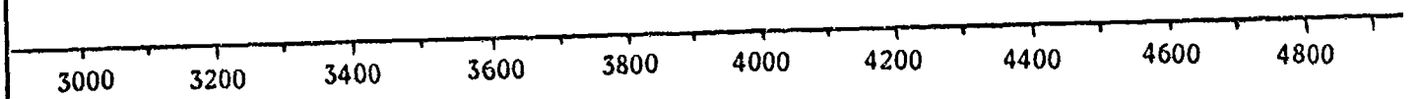

tion of Kerosene/Oxygen Engine at O/F = 6.0 (Central Axis)

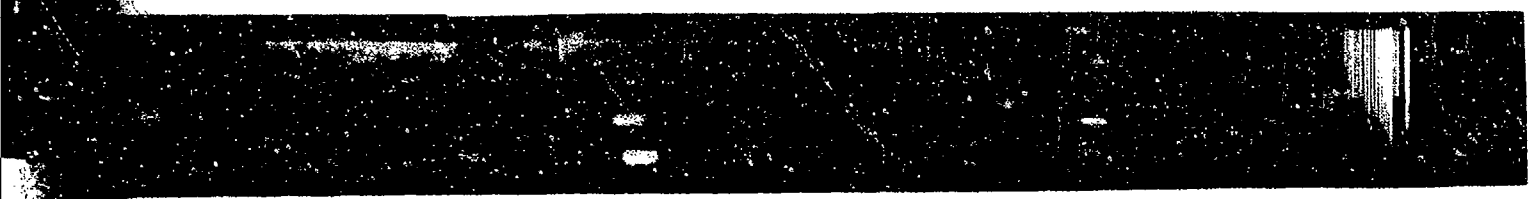

Plume Radiation of Kerosene/Oxygen Engine at O/F = 3.5
ral Axis - Beyond Shock Region)

4800 5000 5200 5400 5600 5800 6000 6200 6400 6600

(The reverse of this page is blank)

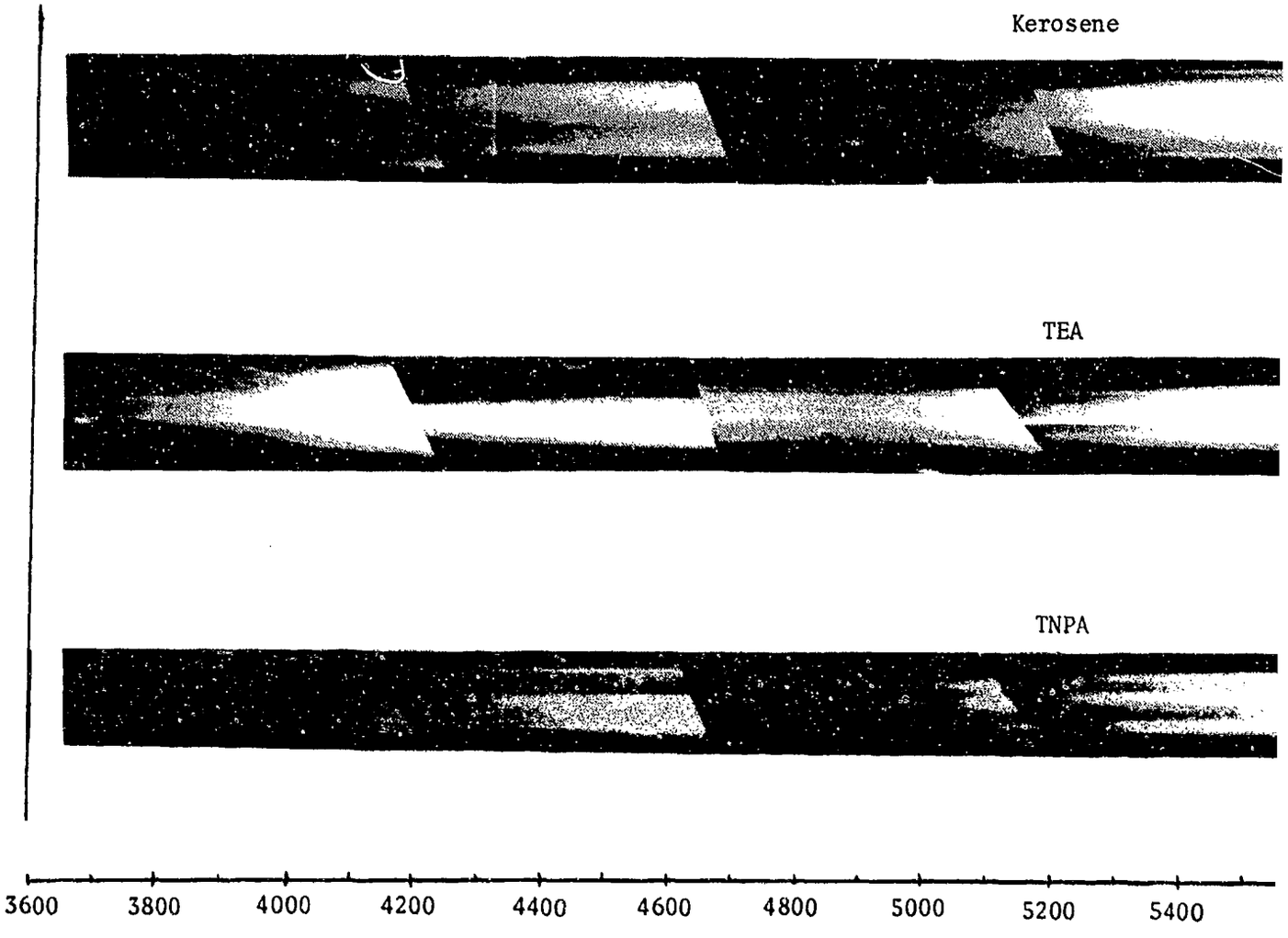

Figure 14. Visible/UV Spectra of Freeburning Ke

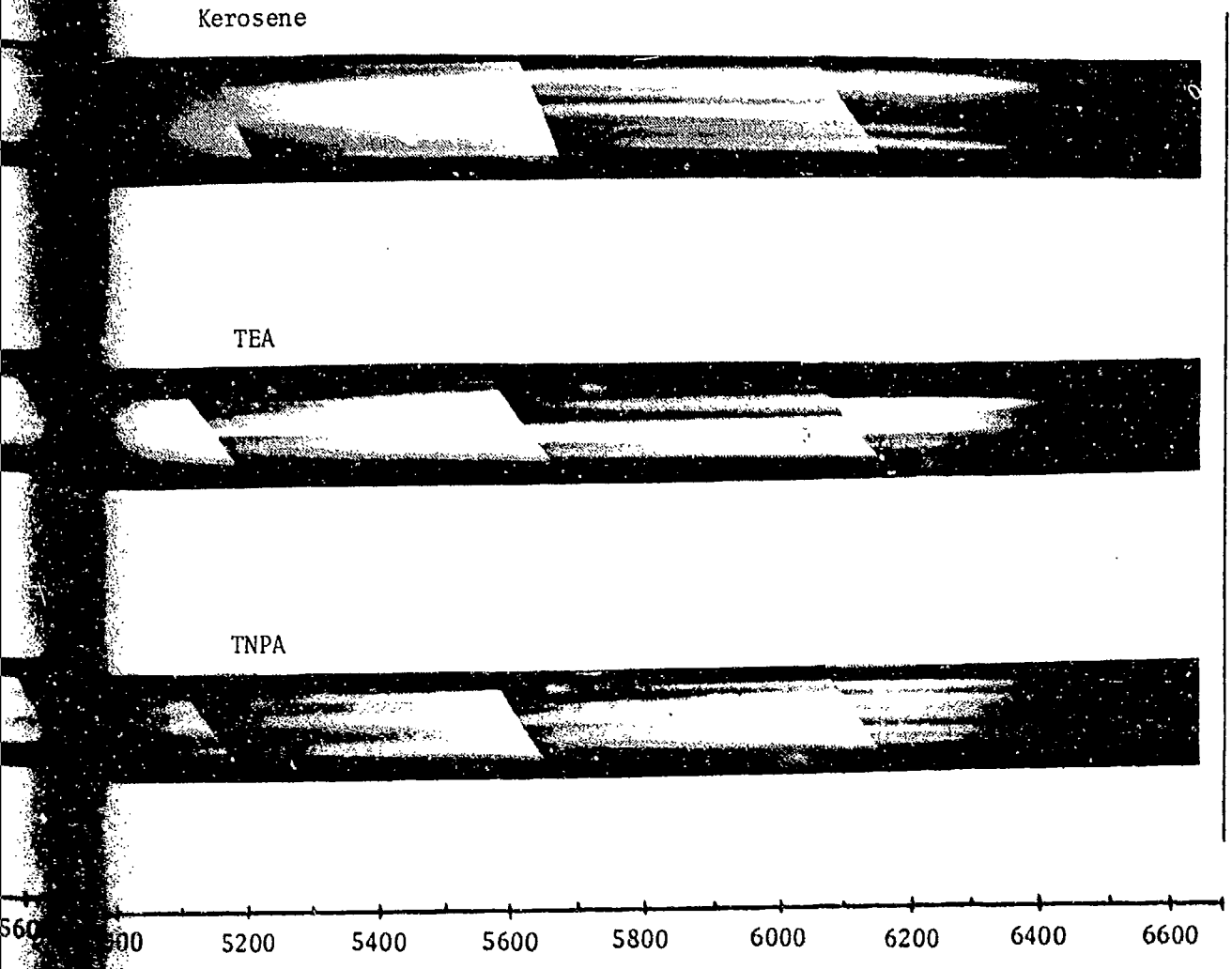

Spectra of Freeburning Kerosene, TEA and TNPA

(The reverse of this page is blank)

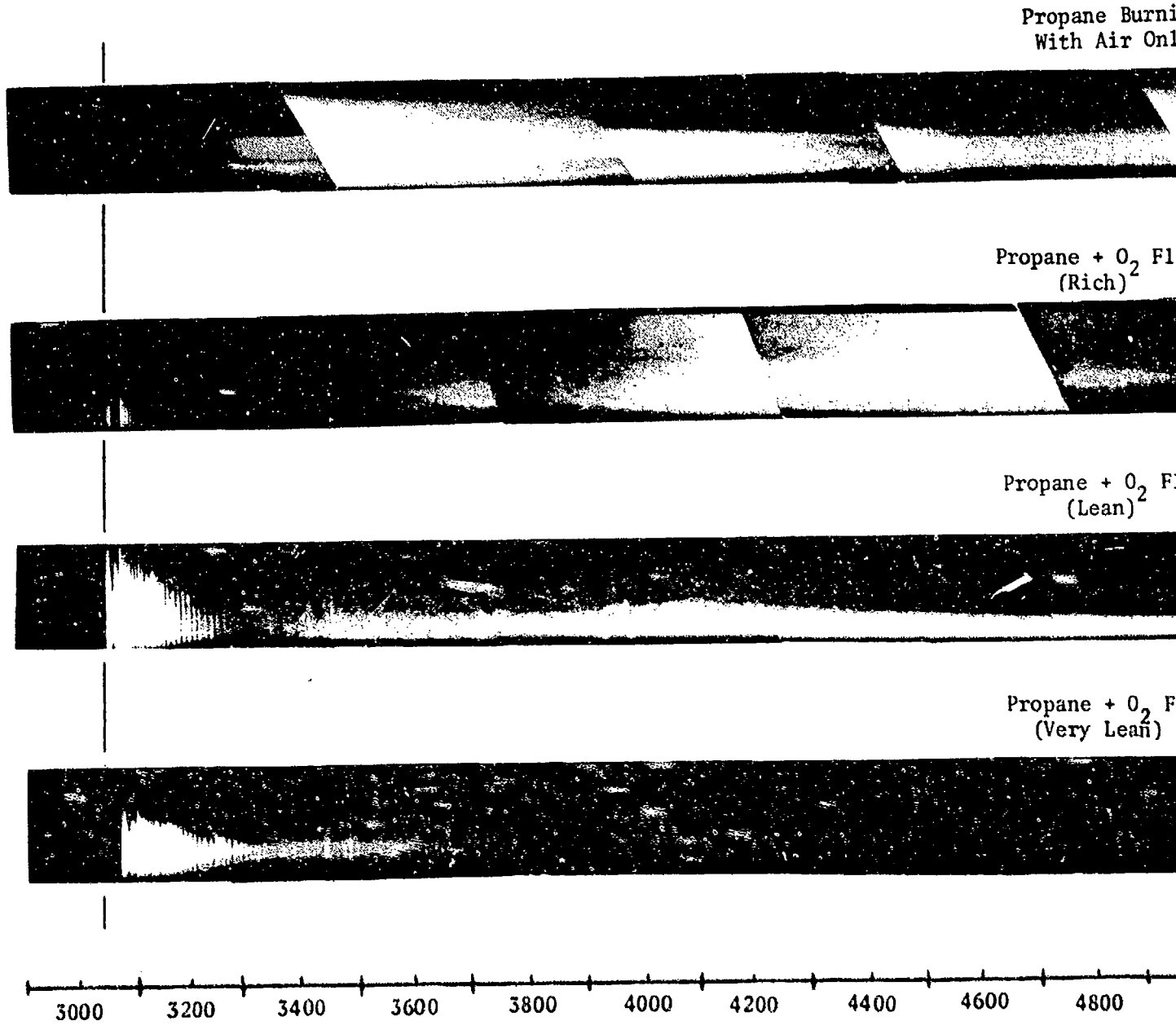

Figure 15. Visible/Ultraviolet Spect

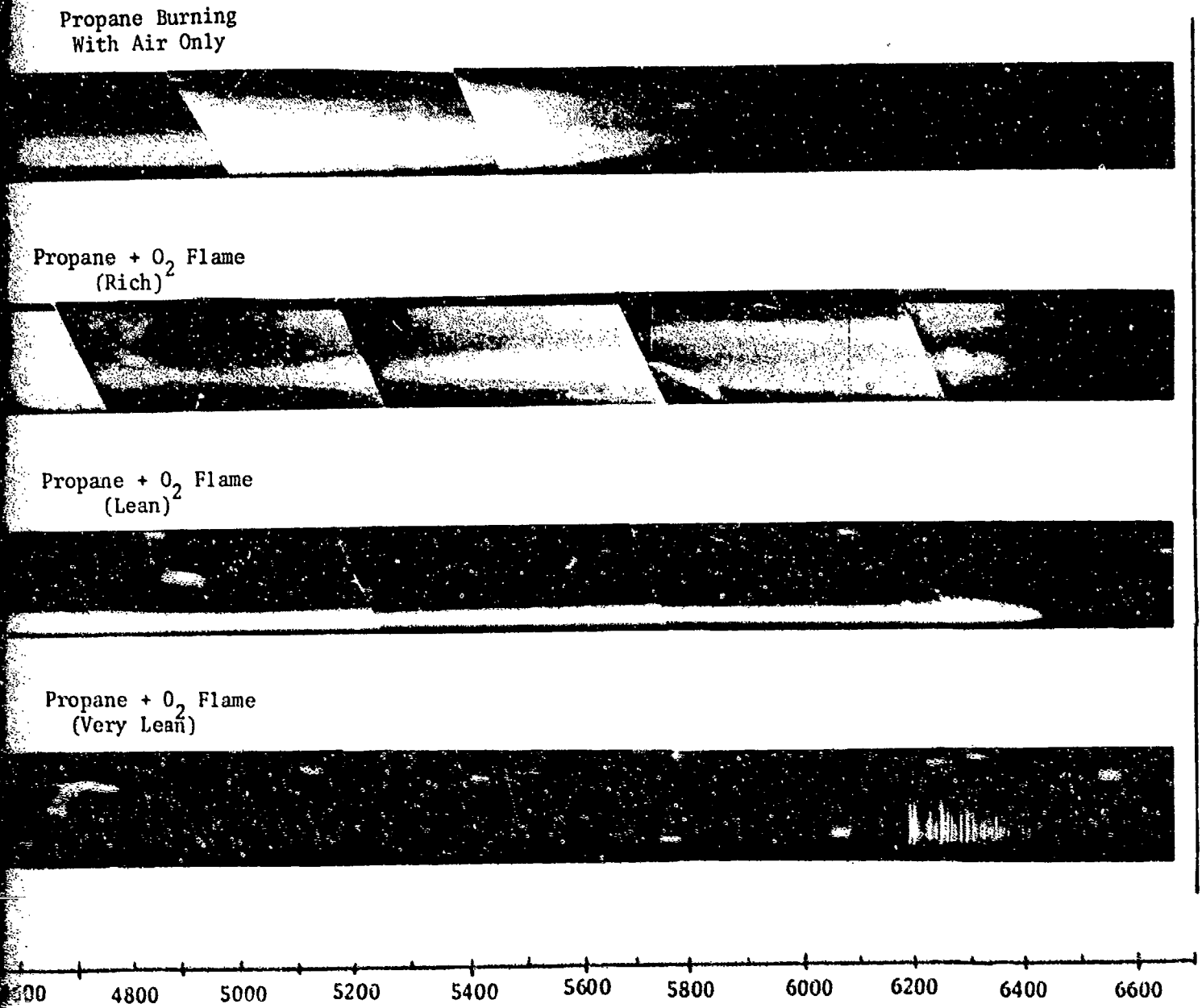

Ultraviolet Spectra of Rich and Lean Propane Flame

(The reverse of this page is blank)

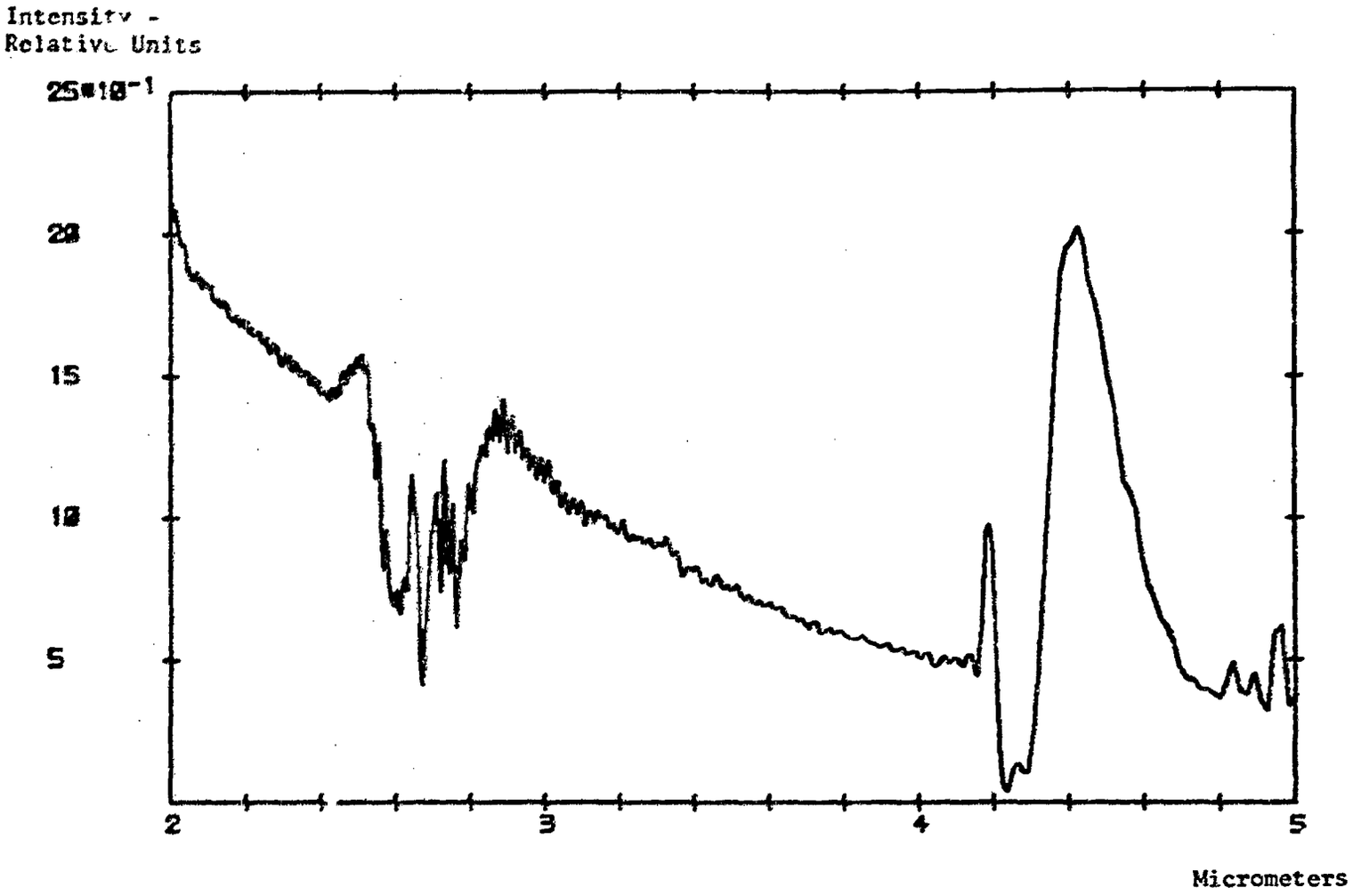

Figure 16. Kerosene Spectrum from 2 to 5 Micrometers (Crucible Burn)

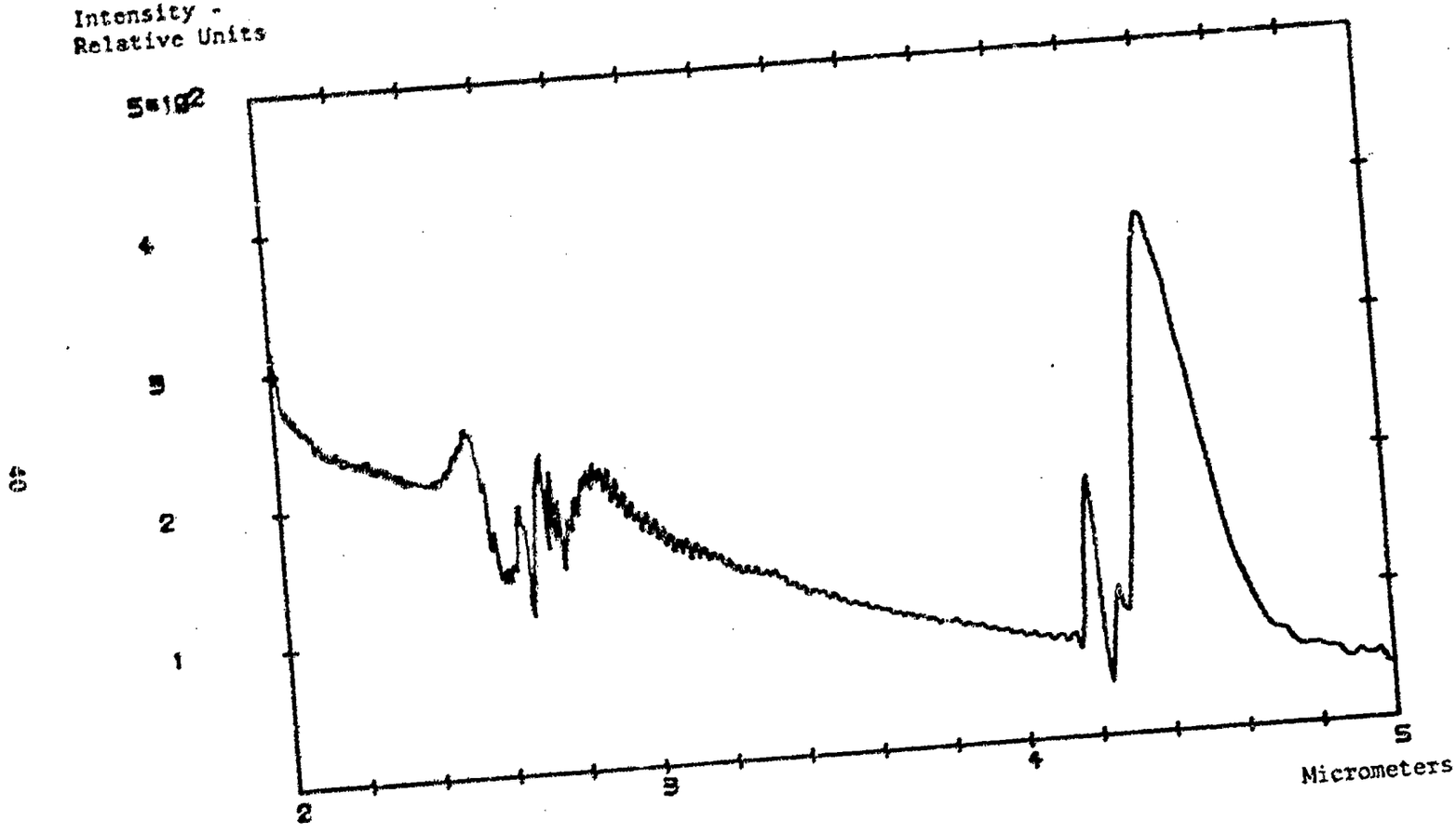

Figure 17. TEA Spectrum from 2 to 5 Micrometers (Crucible Burn)

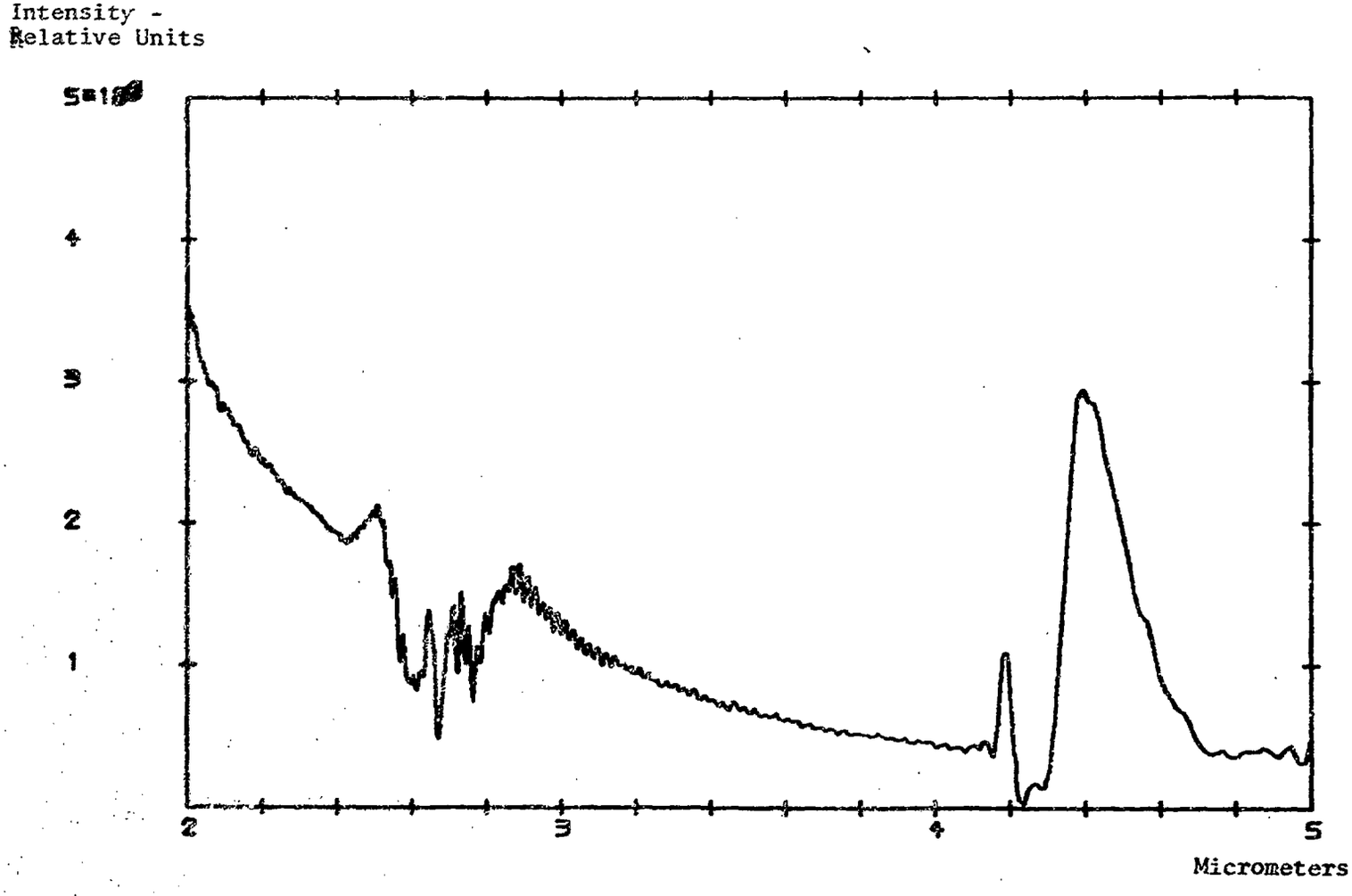

Figure 18. 60% DEAH/40% TEA Spectrum from 2 to 5 Micrometers (Crucible Burn)

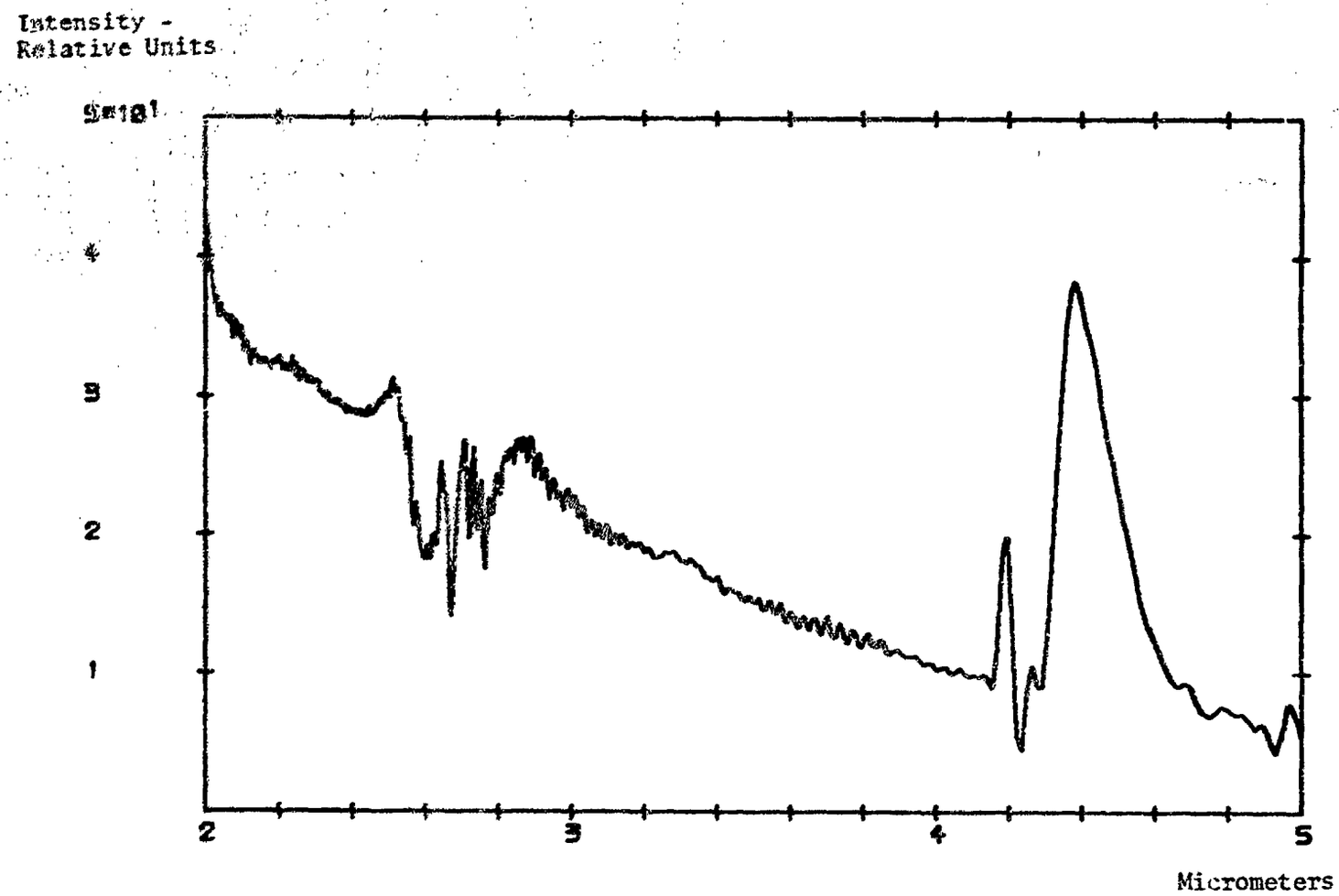

Figure 19. DEAC Spectrum from 2 to 5 Micrometers (Crucible Burn)

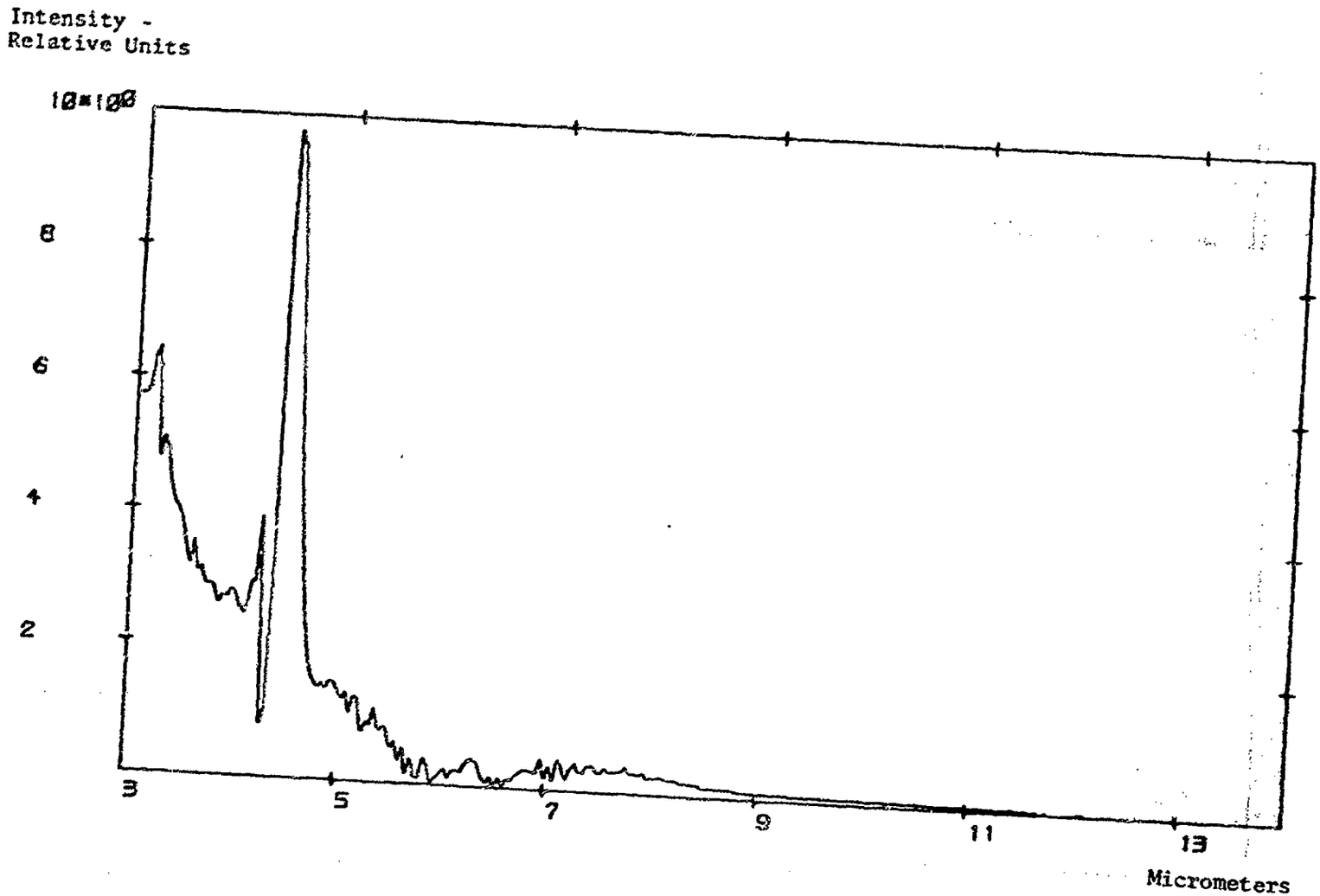

Figure 20. Kerosene Spectrum from 3 to 14 Micrometers (Crucible Burn)

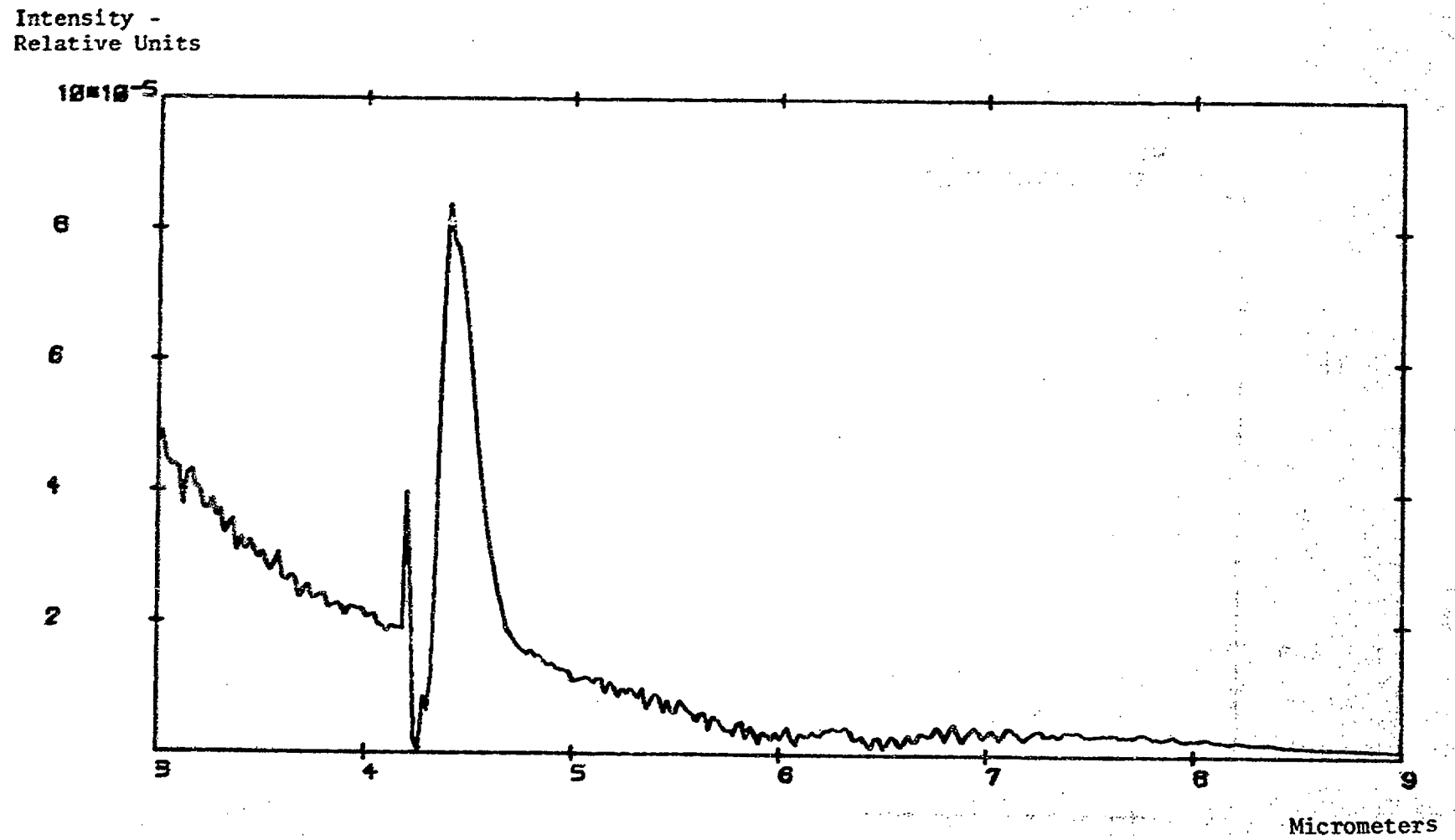

Figure 22. 60% DEAH/40% TEA Spectrum from 3 to 9 Micrometers (Crucible Burn)

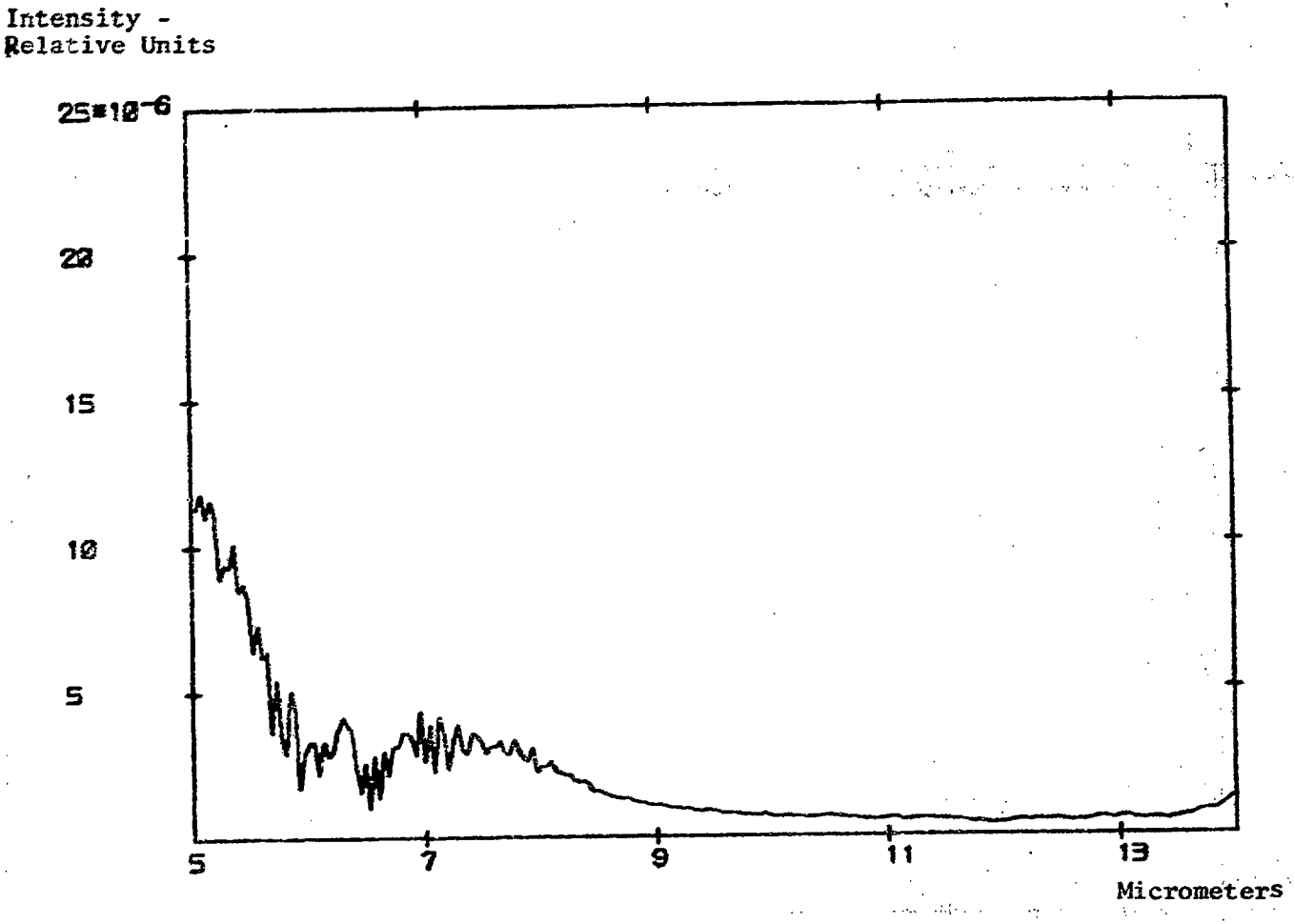

Figure 23. 60% DEAH/40% TEA Spectrum from 5 to 14 Micrometers (Crucible Burn)

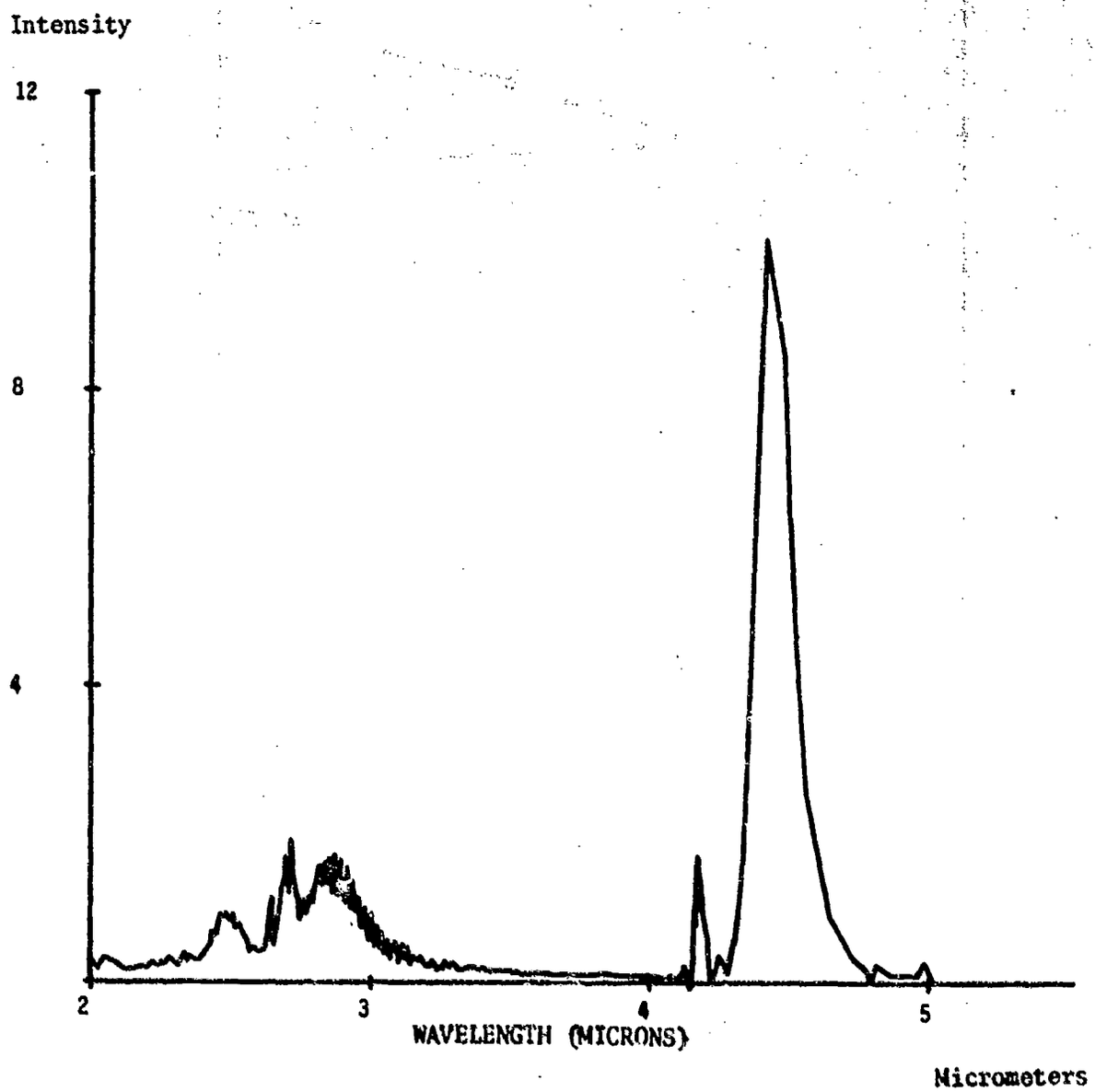

Figure 24. Kerosene/Oxygen Engine Plume Spectra from 2 to 5 Micrometers (O/F = 1.7)

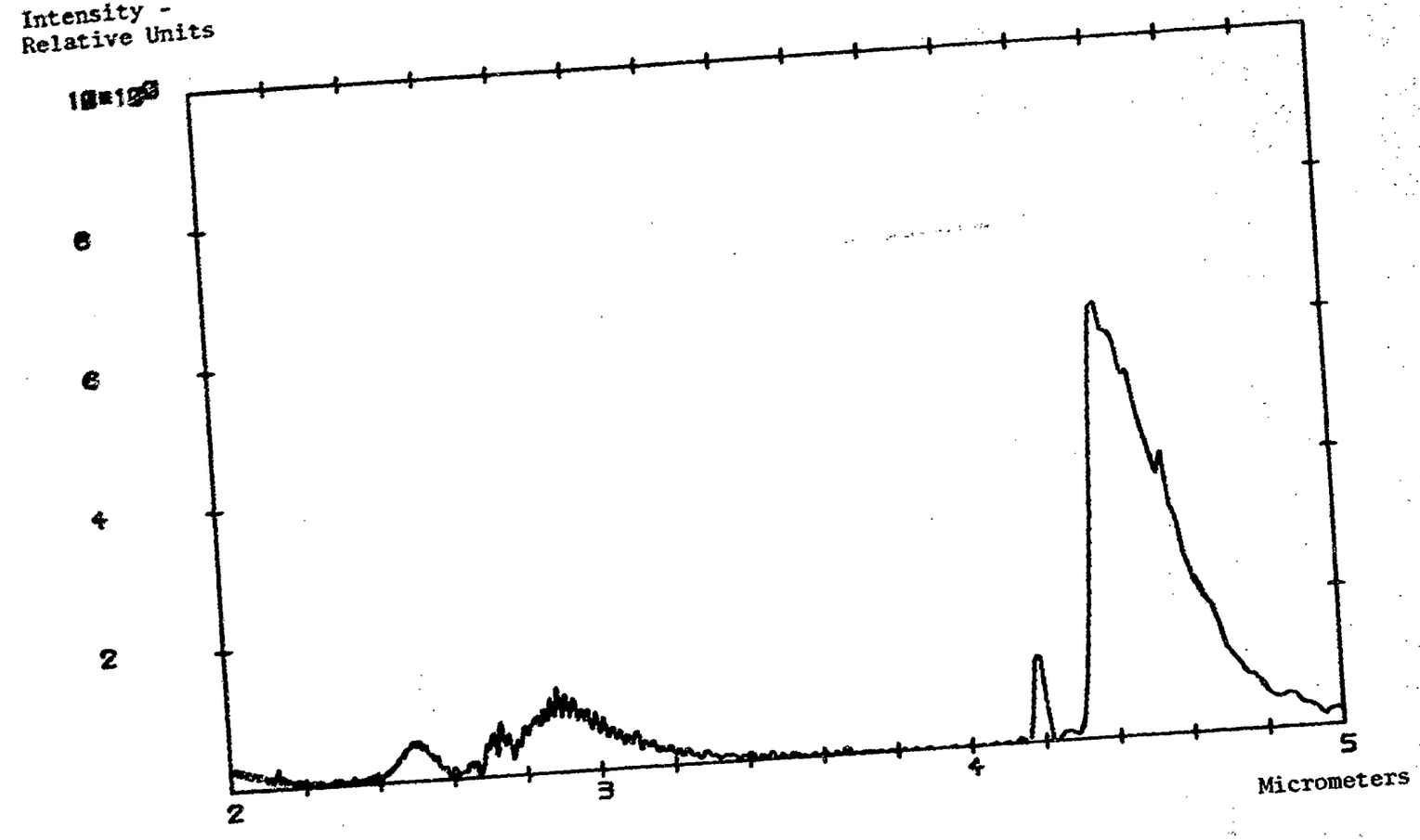

Figure 25. Oxidiser-Rich Spectrum - Propane Torch Emission

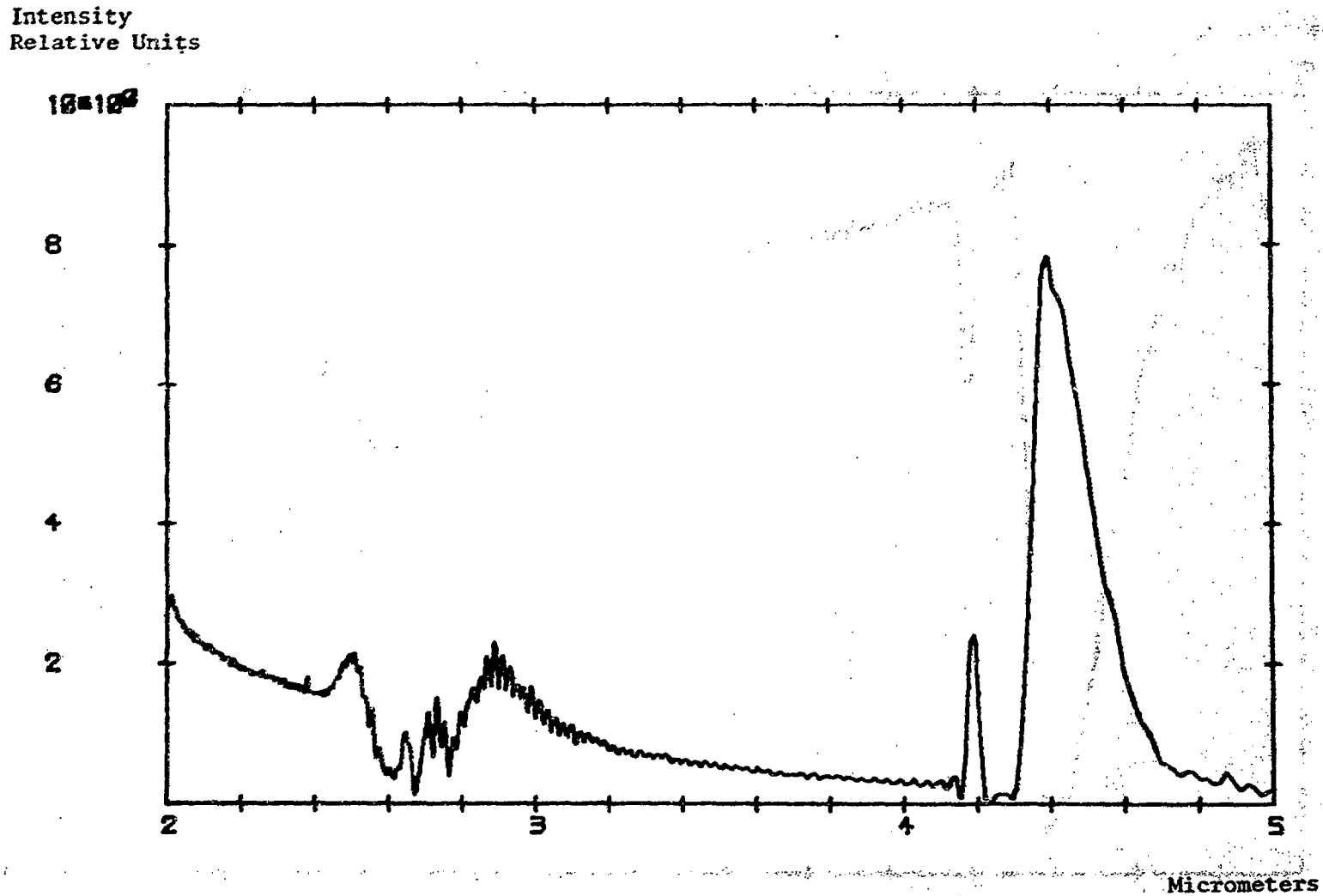

Figure 26. Fuel-Rich Spectrum - Propane Torch Emission

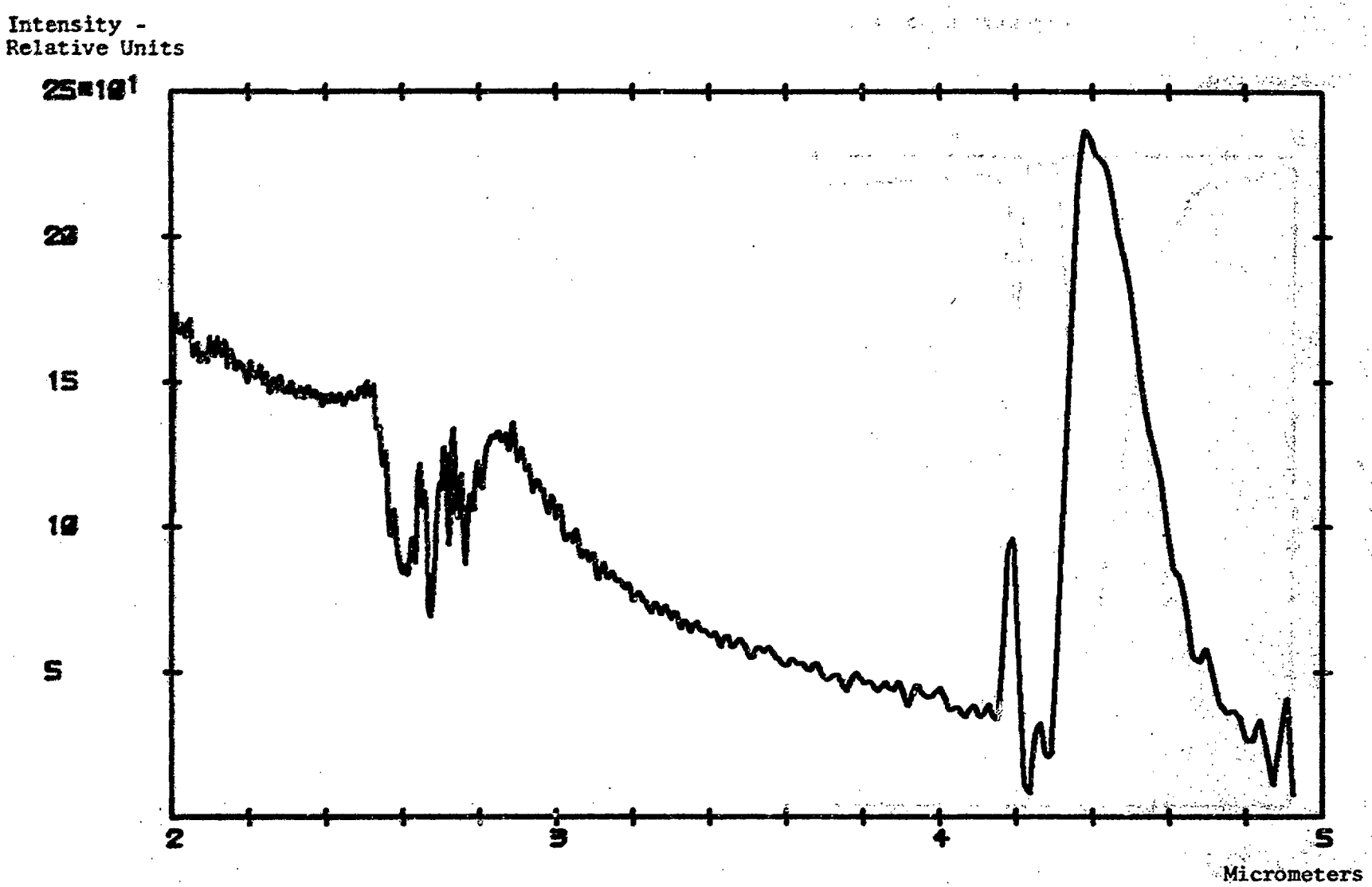

Figure 27. HAST Hybrid Rocker Spectrum from 2 to 5 Micrometers (O/F = 3.0)

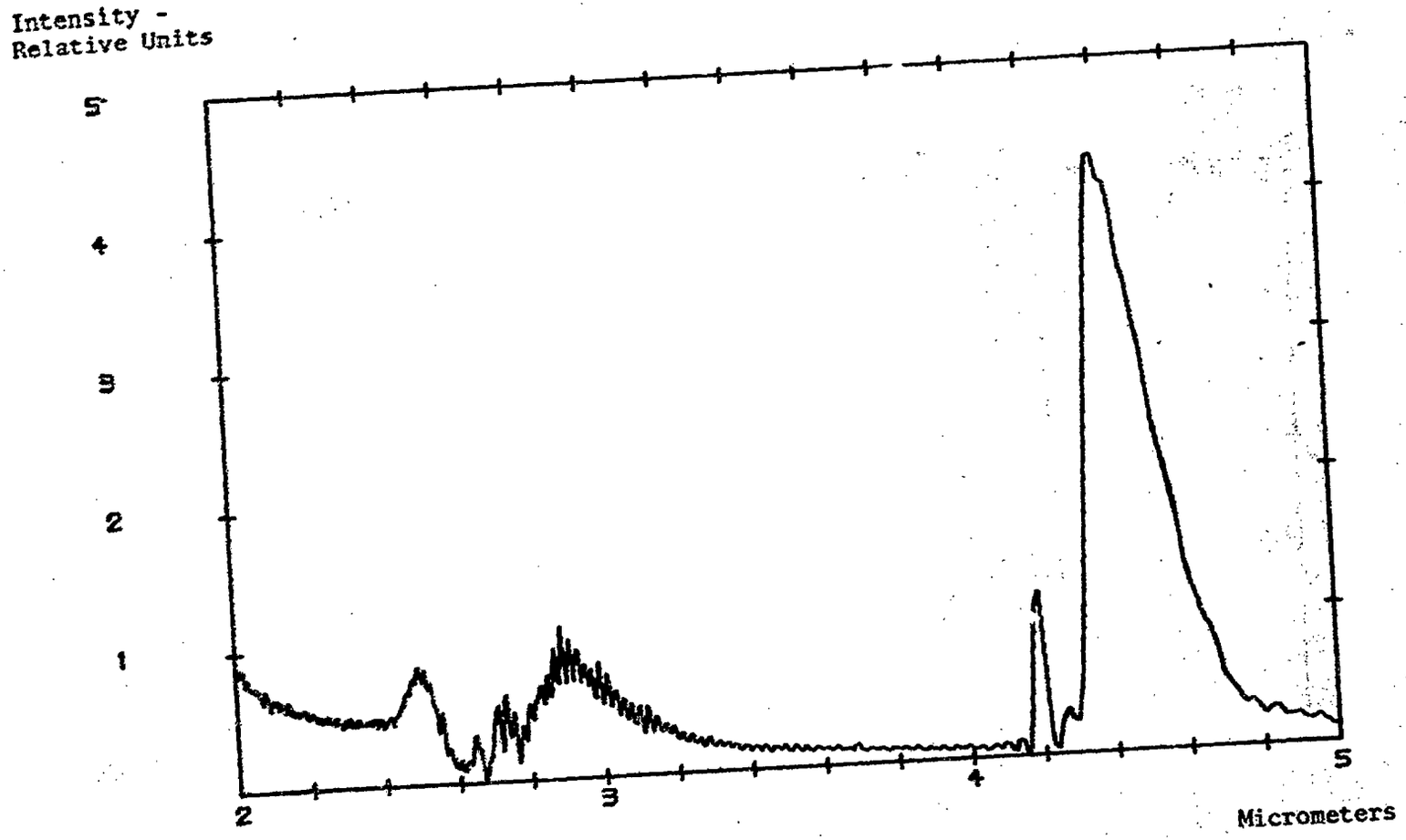

Figure 28. 60% DEAH/40% TEA Spectrum from 2 to 5 Micrometers (Plume Burn - Low Atomization)

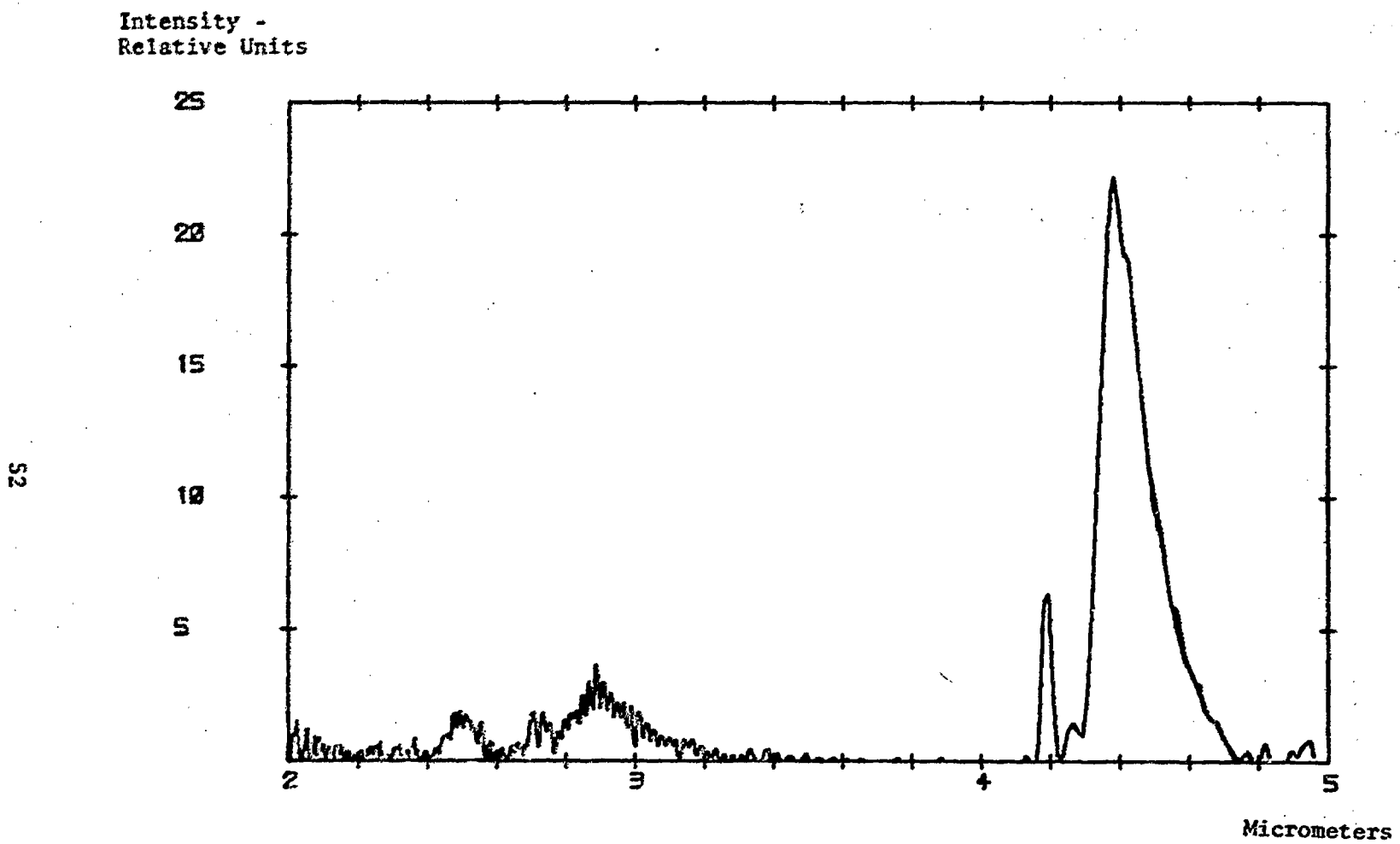

Figure 29. 60% DEAH/40% TEA Spectrum from 2 to 5 Micrometers
(Plume Burn - High Atomization)

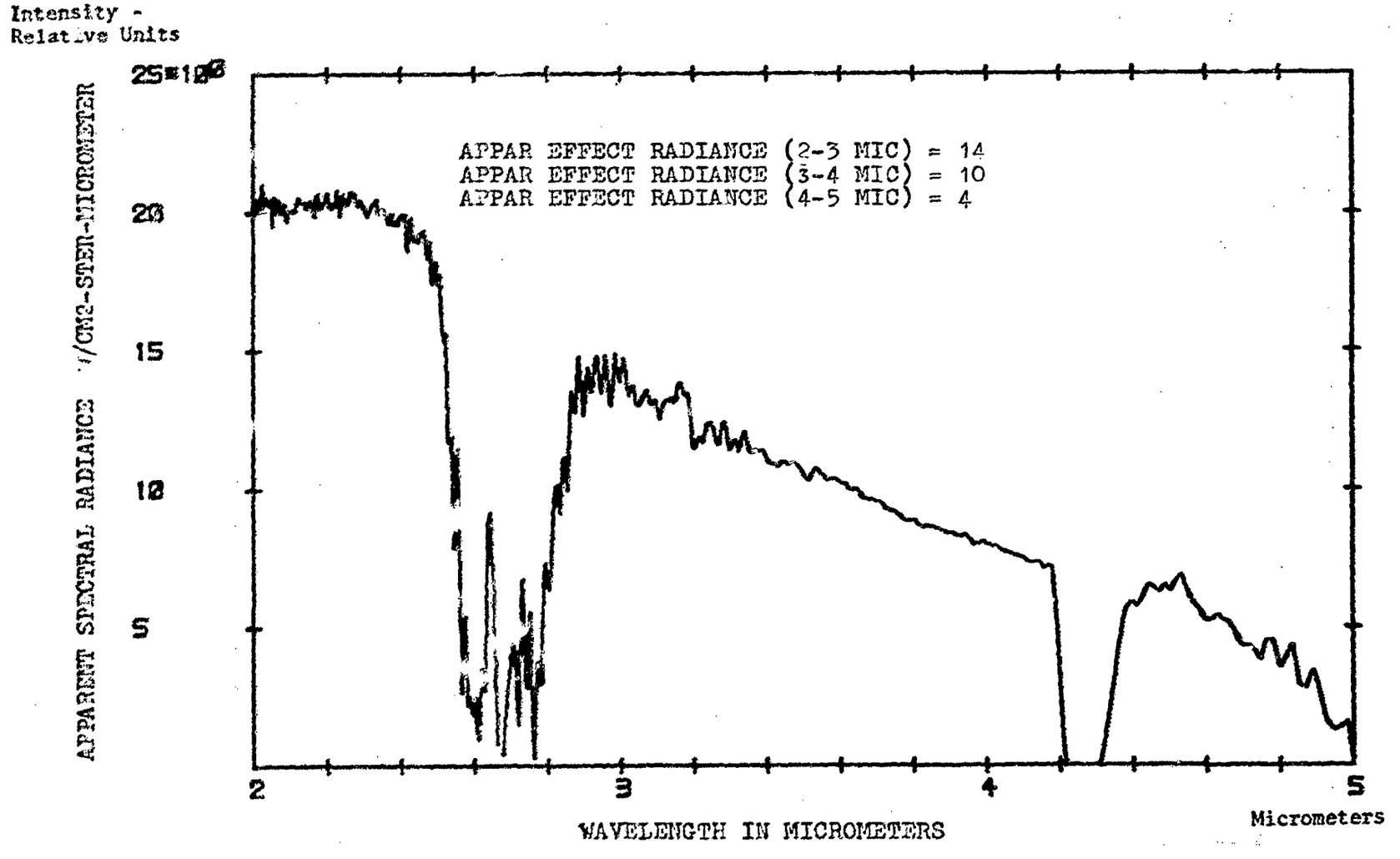

Figure 30. Slurry (Heptane, Sodium Nitrate, Magnesium) Spectrum from 2 to 5 Micrometers - Sea Level

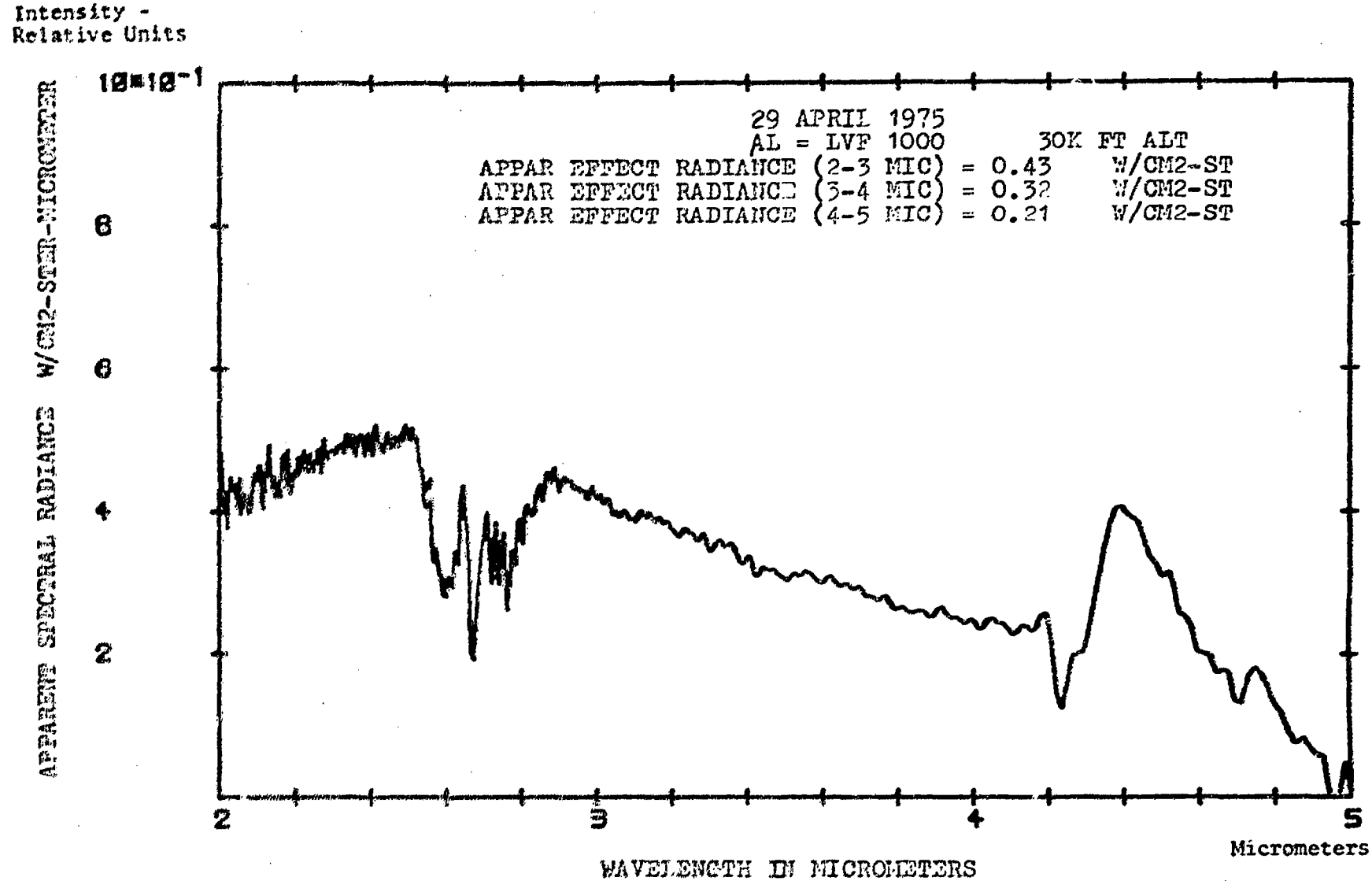

Figure 31. Slurry (Heptane, Sodium Nitrate, Magnesium) Spectrum from 2 to 5 Micrometers - 9.15 Kilometers

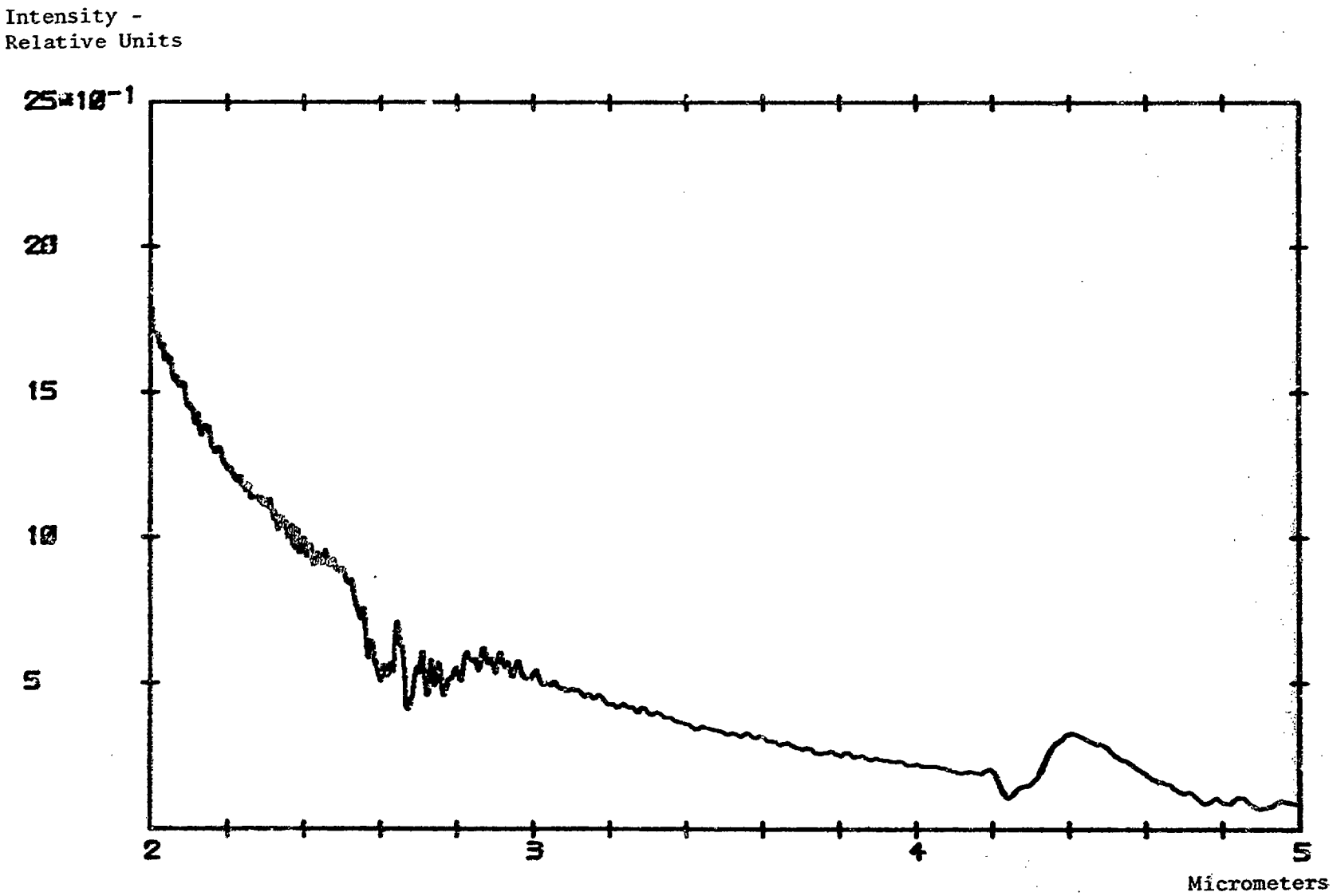

Figure 32. Magnesium/Teflon® Spectrum from 2 to 5 Micrometers - 9.15 Kilometers

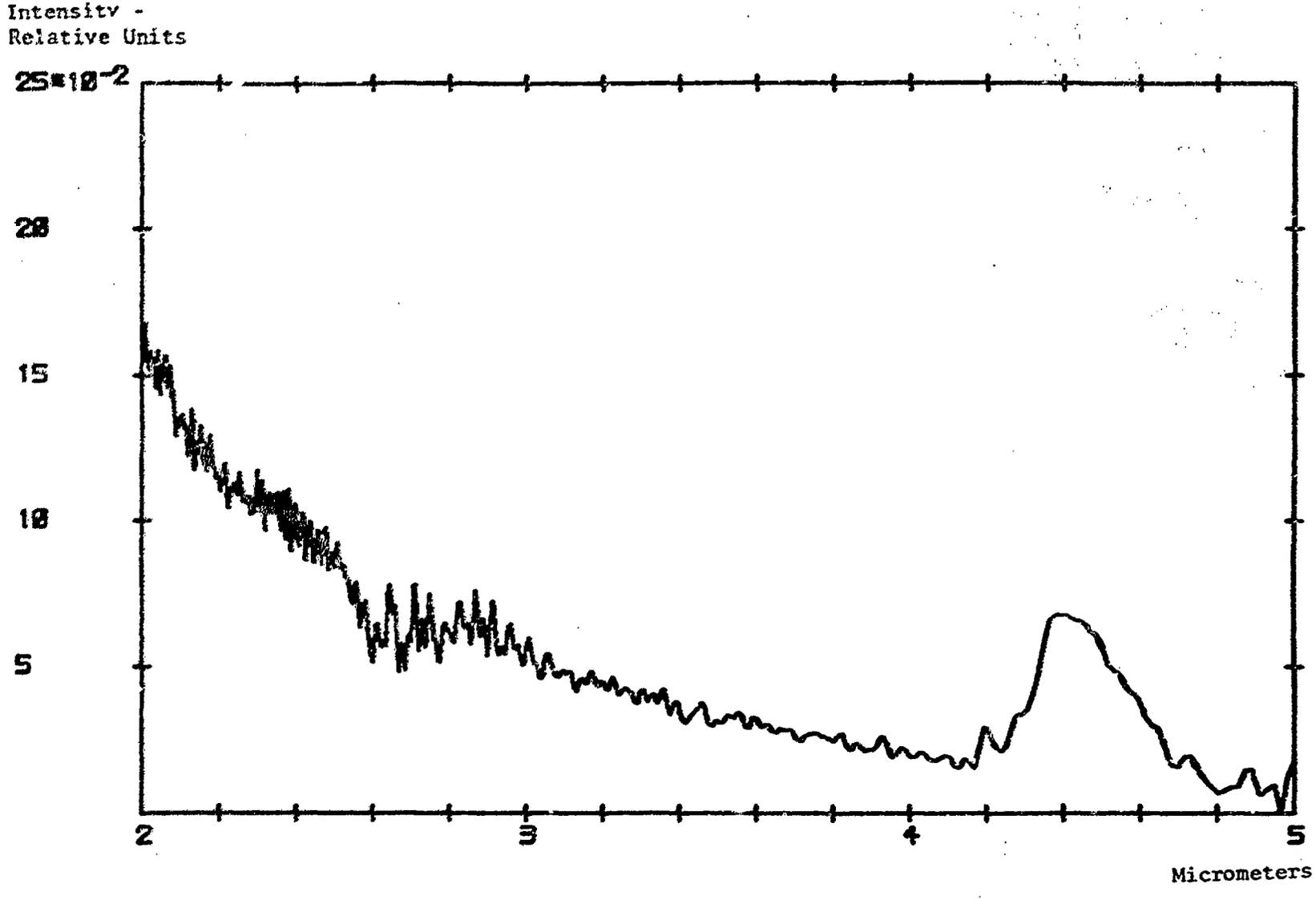

Figure 33. Magnesium/Teflon® Spectrum from 2 to 5 Micrometers - 18.3 Kilometers

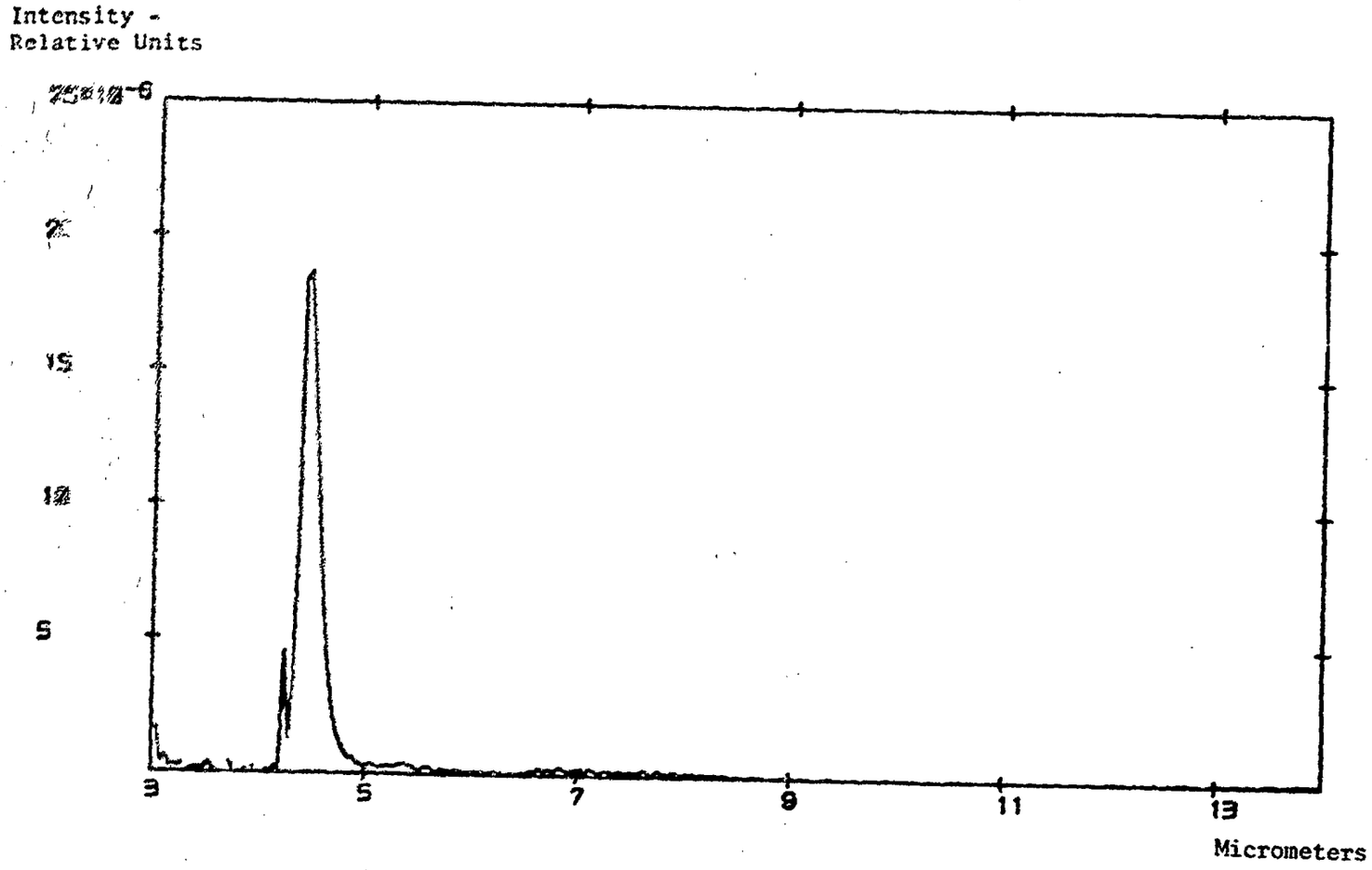

Figure 34. Oxidiser Rich Spectrum from 3 to 14 Micrometers
Propane Torch Emission

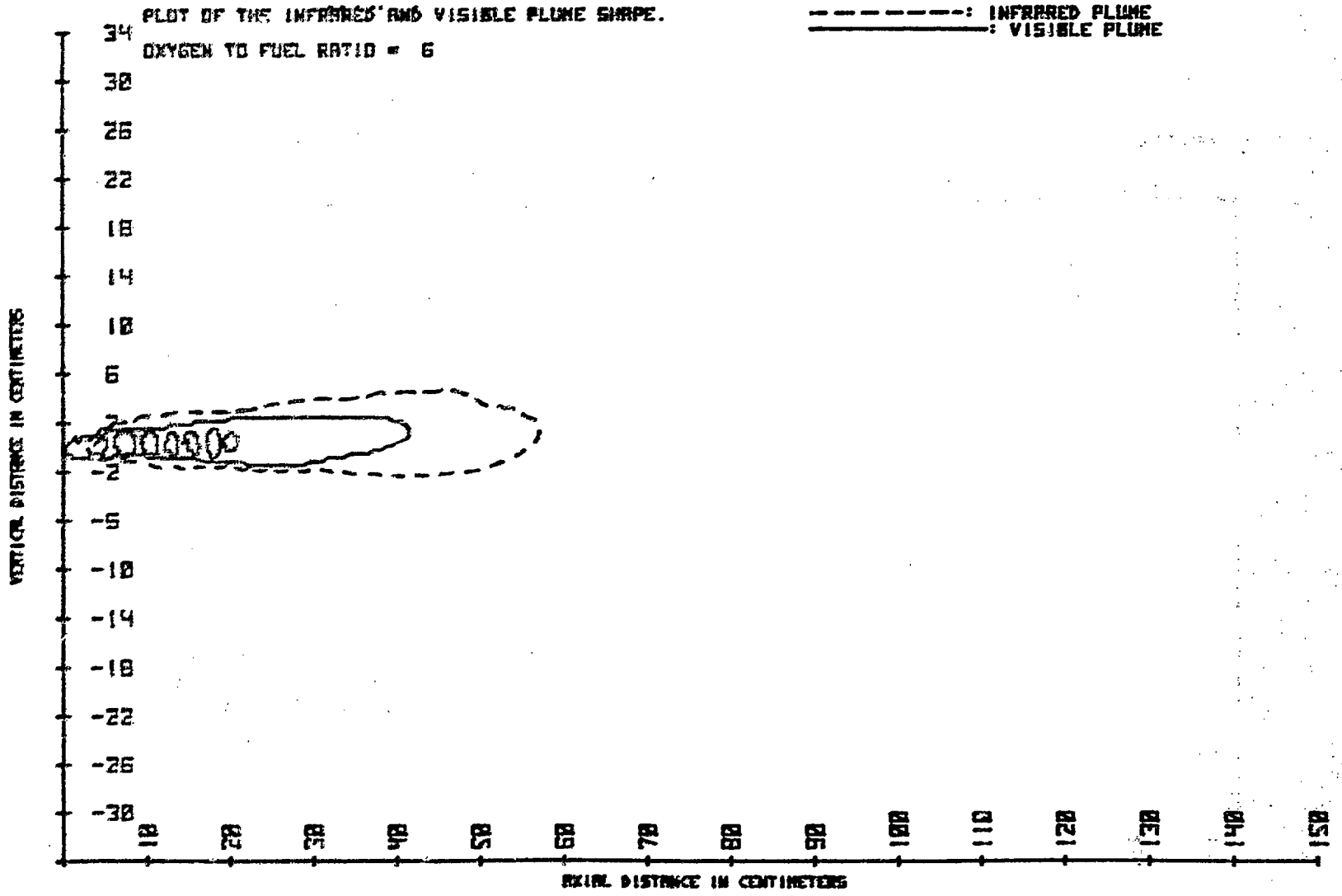

Figure 35. Plot of the Kerosene/Oxygen Engine Infrared and Visible Plume Shape (O/F = 6.0)

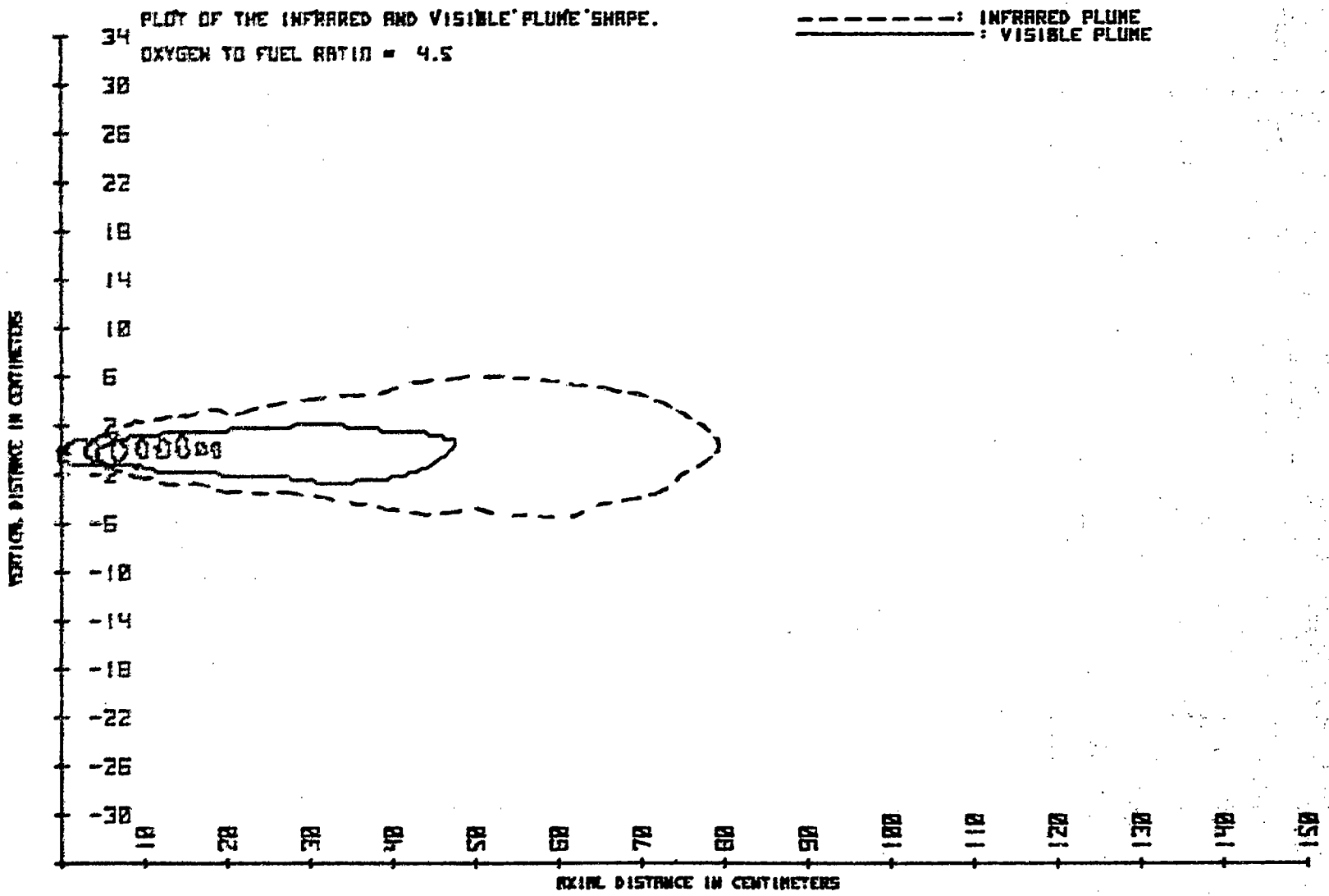

Figure 36. Plot of the Kerosene/Oxygen Engine Infrared and Visible Plume Shape (O/F = 4.5)

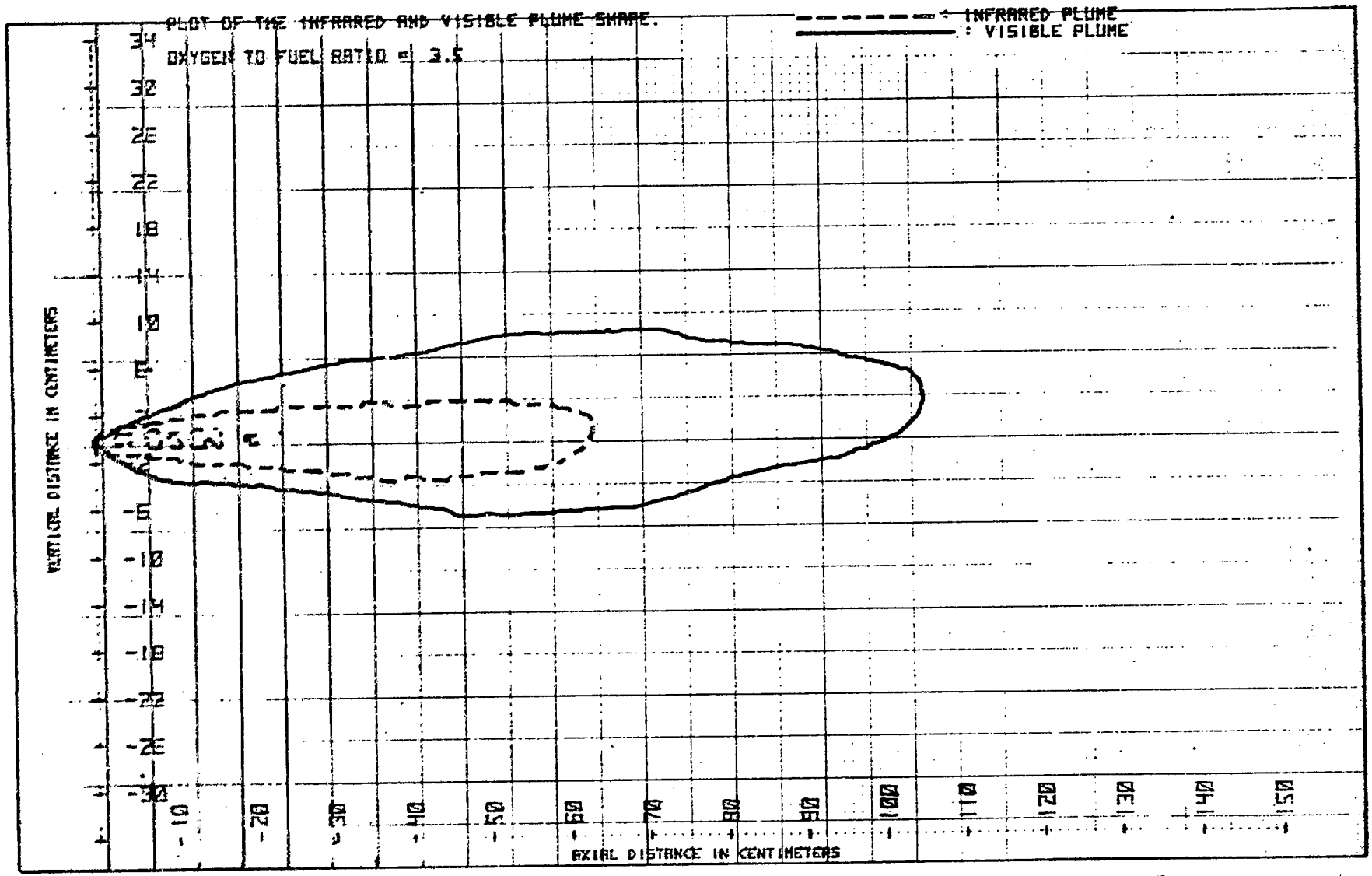

Figure 37. Plot of the Kerosene/Oxygen Engine Infrared and Visible Plume Shape (O/F = 3.5)

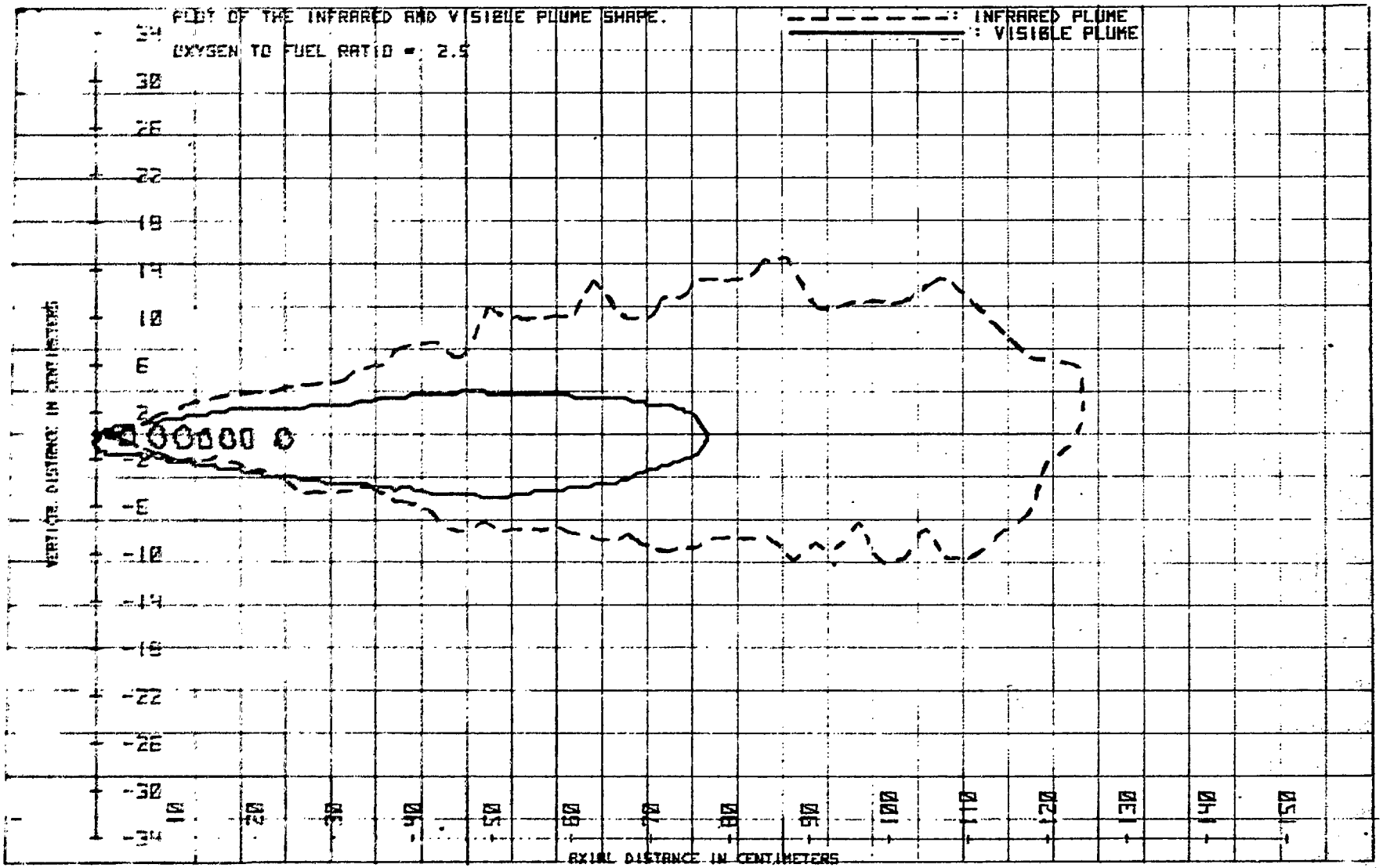

Figure 38. Plot of the Kerosene/Oxygen Engine Infrared and Visible Plume Shape (O/F = 2.5)

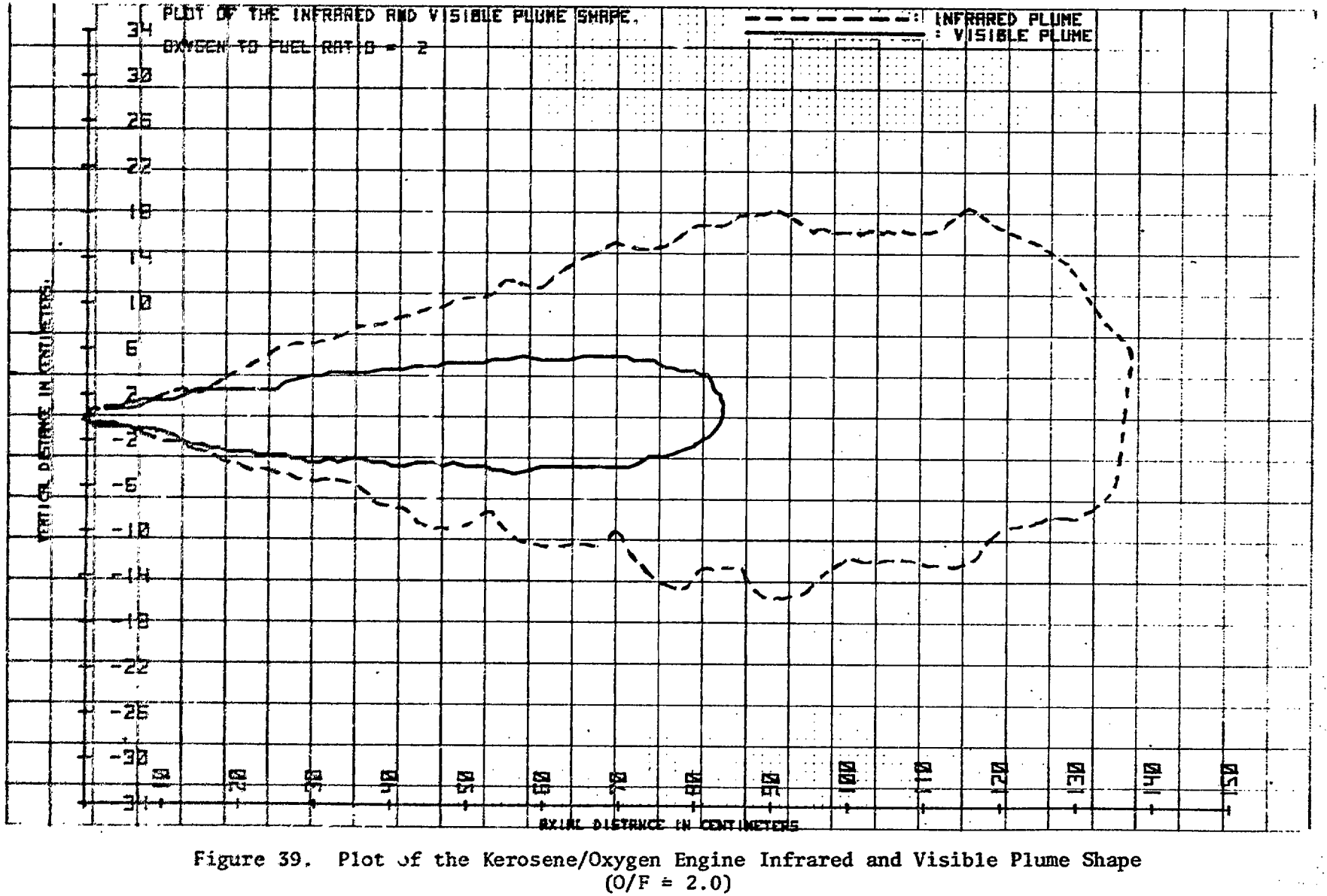

Figure 39. Plot of the Kerosene/Oxygen Engine Infrared and Visible Plume Shape (O/F = 2.0)

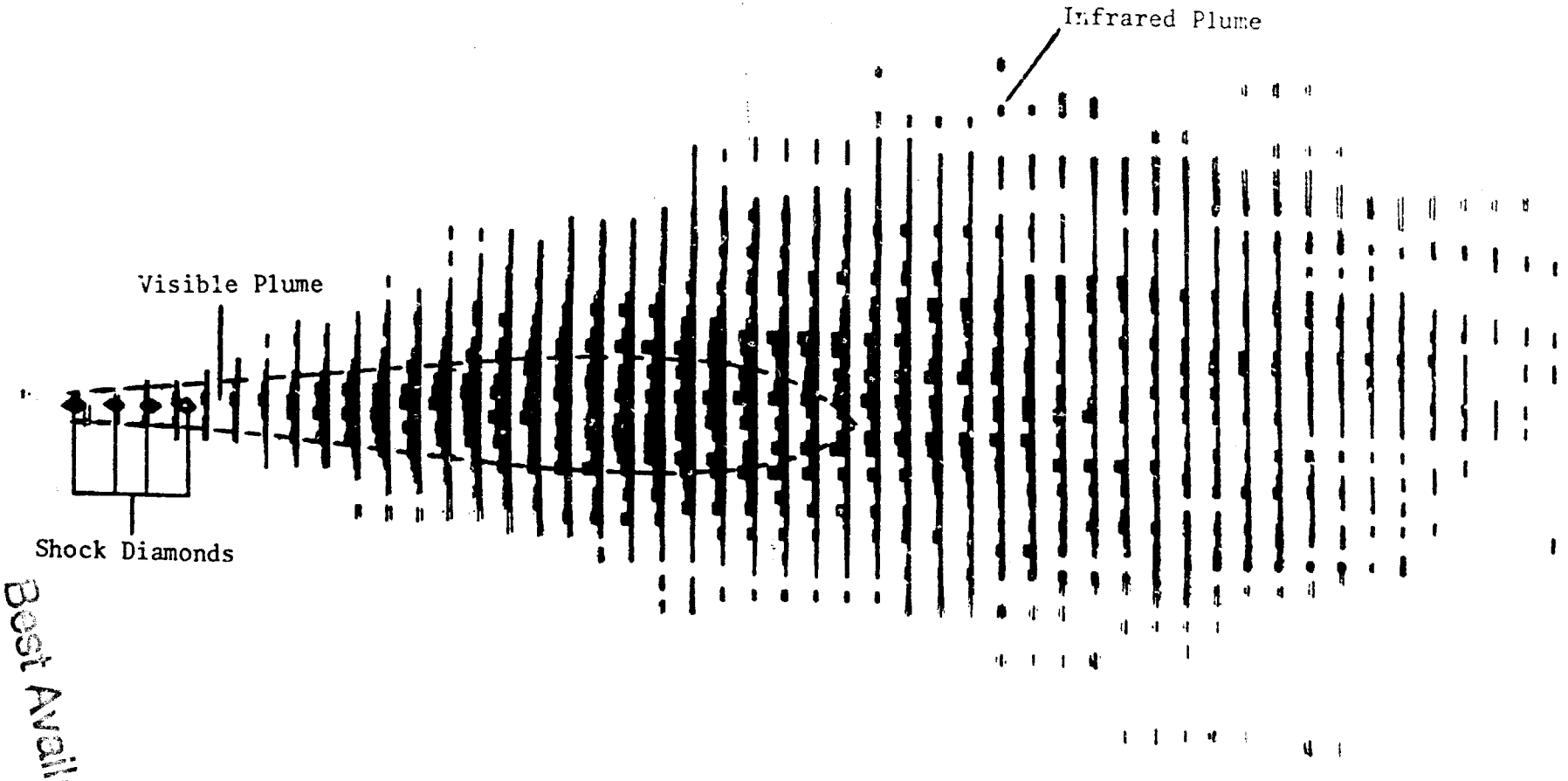

Figure 40. Plot of the Kerosene/Oxygen Engine Infrared and Visible Plume Shape

Best Available Copy

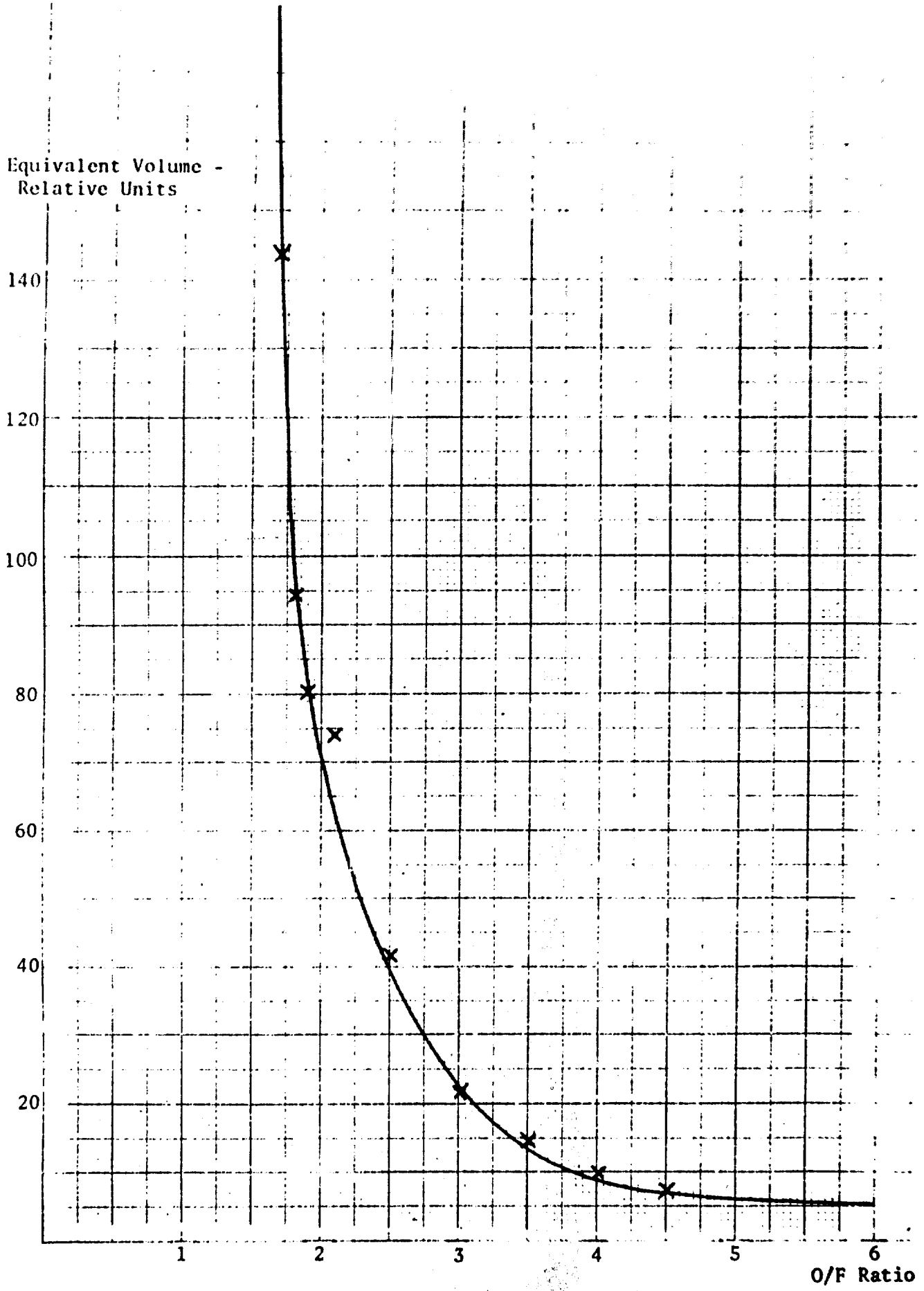

Figure 41. Equivalent Volume of Kerosene/Oxygen Plume Versus O/F Ratio

Best Available Copy

INITIAL DISTRIBUTION

HQ USAF/RDPA	1
HQ USAF/RDQRM	1
HQ USAF/XOOWBQ	1
AFSC/INJ	1
AFSC/SDAS	1
AFSC/SDRA	1
AFSC/DLCAW	2
AFSC/DLC	1
AFSC/SDWA	1
AFSC/DLXP	1
ODDR&E, OSD/COMBAT SUPPORT	1
CIA	1
IDA	1
IDA/LIBRARY	1
IDA	1
AFOSR/NAE	1
FTD/ENDA	1
ASD/XRHP	1
AFAPL/RJT	1
AFCRL	1
AFCRL/LKC	1
AFRPL/DYSP	1
AFRPL/DYSP	1
SANDIA CORP/TECH LIB-3421	1
AEDC (ARO INC./LIB/DOCS)	1
ARO INC	1
USAMICOM/AMSMI-RDK	1
USAMICOM/AMSMI-RDK	1
USAMICOM/AMSMI-REI	1
NMC/CODE 5351	1
NWC/CODE 51	1
NWC/DODE 4513	1
NWC/CODE 5741	1
NWC/CODE 4514	1
NRL/CODE 4004B	1
AEROCHEM	1
AERODYNE	1
AERODYNE	1
AERONAUTICAL RA	1
AEROSPACE CORP	1
AEROSPACE CORP	1
ATLANTIC RESEARCH	1
BEECH ACFT	1
CALSPAN CORP	1
CALSPAN	1
GRUMMAN	1
LOCKHEED	1
LOCKHEED	1
MARTIN MARIETTA	1
PHYSICAL DYNAMICS	1
THIOKOL CORP	1
TRW SYSTEMS	1
UTC	1
BRIGHAM YOUNG UNIV	1
DDC	2
AUL (AUL/LSE-70-239)	1
ASD/ENYS	1
HQ USAF/SAMI	1
HQ 4950 TESTW/TZHM	1
OGDEN ALC/MMNOP	2
AFWL/LR	2
ADTC/TSGPA	1
TAWC/TRADOCLO	1
AFATL/DL	1
AFATL/DLB	1
AFATL/DLM	1
AFATL/DLMQ	20
AFATL/DLOSL	2
UNIV FLORIDA	1
USAMICOM/RGP	1
AVCO SYSTEMS DIV	1
UNIV MARYLAND	1
DARPA	1
AFCRL/OPI	1
ROCKETDYNE	1

Best Available Copy

(The reverse of this page is blank)